J. Fluid Mech. (2000), *vol.* 408, *pp.* 239–274. Printed in the United Kingdom

© 2000 Cambridge University Press

Non-axisymmetric magnetohydrodynamic shear layers in a rotating spherical shell

By ANDREW M. SOWARD[1] AND RAINER HOLLERBACH[2]

[1]School of Mathematical Sciences, University of Exeter, Exeter, EX4 4QE, UK

[2]Department of Mathematics, University of Glasgow, Glasgow, G12 8QW, UK

(Received 3 December 1998 and in revised form 2 August 1999)

Constant-density electrically conducting fluid is confined to a rapidly rotating spherical shell and is permeated by an axisymmetric magnetic field. Slow steady non-axisymmetric motion is driven by a prescribed non-axisymmetric body force; both rigid and stress-free boundary conditions are considered. Linear solutions of the governing magnetohydrodynamic equations are derived in the small Ekman number E limit analytically for values of the Elsasser number Λ less than order unity and they are compared with new numerical results. The analytic study focuses on the nature of the various shear layers on the equatorial tangent cylinder attached to the inner sphere. Though the ageostrophic layers correspond to those previously isolated by Kleeorin *et al.* (1997) for axisymmetric flows, the quasi-geostrophic layers have a new structure resulting from the asymmetry of the motion.

In the absence of magnetic field, the inviscid limit exhibits a strong shear singularity on the tangent cylinder only removeable by the addition of viscous forces. With the inclusion of magnetic field, large viscous forces remain whose strength $\mathscr{Z}$ was measured indirectly by Hollerbach (1994*b*). For magnetic fields with dipole parity, cf. Kleeorin *et al.* (1997), $\mathscr{Z}$ increases throughout the range $\Lambda \ll 1$; whereas, for quadrupole parity, cf. Hollerbach (1994*b*), $\mathscr{Z}$ only increases for $\Lambda \ll E^{1/5}$.

The essential difference between the dipole and quadrupole fields is the magnitude of their radial components in the neighbourhood of the equator of the inner sphere. Its finite value for the quadrupole parity causes the internal shear layer – the Hartmann–Stewartson layer stump – to collapse and merge with the equatorial Ekman layer when $\Lambda = O(E^{1/5})$. Subsequently the layer becomes an equatorial Hartmann layer, which thins and spreads polewards about the inner sphere surface as Λ increases over the range $E^{1/5} \ll \Lambda \ll 1$. Its structure for the stress-free boundary conditions employed in Hollerbach's (1994*b*) model is determined through matching with a new magnetogeostrophic solution and the results show that the viscous shear measured by $\mathscr{Z}$ decreases with increasing Λ. Since $\mathscr{Z}$ depends sensitively on the detailed boundary layer structure, it provides a sharp diagnostic of new numerical results for Hollerbach's model; the realized $\mathscr{Z}$-values compare favourably with the asymptotic theory presented.

1. Introduction

1.1. *General remarks*

In recent years, there has been considerable progress in our understanding of the geodynamo problem. The numerical modelling has reached a stage at which comparisons can be made with observational data. At its simplest level the Earth's fluid core

https://doi.org/10.1017/S0022112099007776 Published online by Cambridge University Press

is a rapidly rotating spherical shell (constant rotation rate $\boldsymbol{\Omega}^*$) filled with electrically conducting fluid in slow relative motion. Motion is driven by buoyancy forces, which may be either thermal or compositional. As a consequence of the rotational constraints in the small Ekman number limit ($E \ll 1$, see (1.1) below), such convection is generally non-axisymmetric. Through nonlinear mechanisms axisymmetric flows can also be generated possibly through thermal winds and Lorentz forces. The geodynamo problem concerns both the generation of the magnetic field permeating the fluid by magnetic induction as well as the back reaction of the magnetic field on the flow by the Lorentz force. Recent reviews are given by Hollerbach (1996*a*) and Fearn (1997).

All recent fully three-dimensional numerical integrations of convection-driven geodynamo models (including Glatzmaier & Roberts 1995*a*, *b*, 1996*a*, *b*, 1997; Kuang & Bloxham 1997, 1999; Christensen, Olson & Glatzmaier 1998; Kitauchi & Kida 1998; Sarson, Jones & Longbottom 1998; Sakuraba & Kono 1999; Sarson & Jones 1999) have drawn attention to the importance of the tangent cylinder with generators parallel to the rotation axis, which touches the inner core at its equator. This is because the rotational constraints, imposed as a consequence of the Proudman–Taylor theorem, cause the convection above and below the inner solid core, inside the tangent cylinder, to have a different character to that outside the tangent cylinder (Busse & Cuong 1977). It is also a consequence of these differences that the nonlinearly excited axisymmetric flows exhibit similar differences. This is evident, for example, in the numerical integrations of axisymmetric mean field models (Anufriev & Hejda 1998, 1999).

In view of the partitioning of the flow by the tangent cylinder into an interior *polar* region and an exterior *equatorial* region, some complicated shear layer structure is to be expected on the tangent cylinder itself. Such axisymmetric shear layers have been studied largely within the context of small differences of the angular velocity between the solid inner core and outer rigid mantle. Glatzmaier & Roberts' (1995*a*) numerical geodynamo simulations indicated super-rotation of the inner core which was subsequently confirmed by seismic data (Song & Richards 1996). One possible explanation of the mechanism has been given by Aurnou, Brito & Olson (1996).

Hollerbach (1996*b*) undertook an analytic investigation of the MHD shear layers due to boundaries in relative motion in a simplified plane layer geometry in the spirit of Stewartson's (1957) pioneering non-magnetic study. Numerical studies in the true spherical shell geometry with an applied axial dipole magnetic field by Hollerbach (1994*a*) and Dormy, Cardin & Jault (1998) reveal a rich boundary layer structure, which is partially explained by Hollerbach's (1996*b*) results. Further clarification followed from Kleeorin *et al.*'s (1997) (subsequently referred to as K-S) asymptotic analysis of the shear layers in the spherical shell; this provided the MHD extension of Stewartson's (1966) seminal paper.

As a preliminary step towards understanding non-axisymmetric shear layers, Hollerbach & Proctor (1993) assumed that the buoyancy force which drives convection is prescribed rather than determined as the solution of the heat conduction equation. They then considered the non-axisymmetric flow driven by that non-axisymmetric force alone. In terms of our dimensionless units of § 1.2, they found the velocity $\boldsymbol{u}$ driven by the force $\boldsymbol{f}$ that solves the inhomogeneous geostrophic balance equation

$$2\hat{\boldsymbol{z}}\times\boldsymbol{u} = -\nabla p + \boldsymbol{f} \quad (\nabla\cdot\boldsymbol{u} = 0).$$

Though it is known that such non-axisymmetric flows are unique (Greenspan 1968), they unexpectedly found that the flow generally exhibits singular behaviour mani-

https://doi.org/10.1017/S0022112099007776 Published online by Cambridge University Press

fested as jets on the tangent cylinder. This must be contrasted with the axisymmetric case for which motion is determined up to the addition of an arbitrary axisymmetric geostrophic flow and then only when the azimuthal couple produced by the force on geostrophic cylinders vanishes. In the MHD context this is known as Taylor's condition (1963).

Evidently the singularity on the tangent cylinder may be removed by the addition of viscous effects. Nevertheless, this leaves shear layers whose intensity increases as the Ekman number decreases to zero ($E \downarrow 0$). Hollerbach (1994*b*) (subsequently referred to as H94) considered the alternative possibility that with the inclusion of a magnetic field the Lorentz force can remove the singularity. He therefore considered numerically, for various small values of E, the influence of an applied magnetic field of moderate strength as measured by the Elsasser number Λ (see (1.1) below). Certainly his evidence for Λ of order unity and larger suggested that the magnetic field has a smoothing influence.

In this paper we investigate H94's problem analytically at small Elsasser number. Perhaps the most striking feature of our results is that, with increasing field strength at fixed small E, the tangent-cylinder shear layers intensify until Λ achieves a sufficiently large value at which all trace of internal (as opposed to boundary) viscous layers has evaporated. The analysis closely parallels the earlier study by K-S. Many of the parameter ranges and boundary layer structures identified in K-S have their counterparts here; nevertheless, there are important non-trivial differences that emerge from the non-axisymmetry. Essentially, the most pronounced effect at small Elsasser number $1 \ll \Lambda \ll E^{1/3}$ is the two-dimensionality imposed by geostrophy. It means that the singular behaviour triggered at the inner sphere equator is transmitted over the entire tangent cylinder. Though the magnetic field leads to significant smoothing of the zonal shear flow velocity, when $E^{1/2} \ll \Lambda$, in relatively large magnetotopographic and magnetogeostrophic regions, considerable gradients of the shear remain in viscous sublayers, whose radial length scale decreases with increasing Λ so exacerbating the shear singularity. For $E^{3/7} \ll \Lambda \ll E^{1/3}$, the viscous region is dominated by a Hartmann layer covering the entire tangent cylinder. While for $\Lambda \gg E^{1/3}$ it detaches from the outer sphere and becomes a Hartmann–Stewartson layer stump attached to the equator of the inner-sphere. It is only after the stump has shrunk completely into the inner-sphere Ekman–Hartmann boundary layer that the intensity of the tangent cylinder shear, as measured by $\mathscr{Z}$ (see (1.9) below), begins to decrease.

Though our analytic results are compatible with H94's numerics at the relatively large values of Λ employed there, further numerical results at smaller Elsasser number are presented here to support the trends predicted by our theory. The central difficulty in making any quantitative comparison is the extremely small values of E and Λ necessary for the validity of the asymptotics. Nevertheless, we clearly identify the nature of the mechanisms which characterize the transition from increasing to decreasing $\mathscr{Z}$ on the tangent cylinder. The isolation of these processes is central to our understanding of the role of the tangent cylinder in Earth's core dynamics.

We remark that the numerical results presented here and in H94 assume that the region outside the shell is an electrical insulator, but note that none of our analytic results depend on the electrical conductivity of the boundaries correct to the order taken. This is in stark contrast to the axisymmetric flow driven by differentially rotating the inner and outer spheres, for which any interior motion depends on viscous and electromagnetic coupling with the boundary. In that case, it is well known that the resulting flow for insulating and perfectly conducting boundaries is very different. The reason why our asymmetric motions are insensitive is that they respond directly

https://doi.org/10.1017/S0022112099007776 Published online by Cambridge University Press

to the applied body force and any dependence on boundary conductivity is restricted to low-order features of the surface boundary layers.

1.2. *Mathematical formulation*

Relative to the frame rotating with angular velocity $\boldsymbol{\Omega}^*$ in which the shell is at rest, asymmetric steady flow velocity $U^*\boldsymbol{u}$ is forced by the body force $\Omega^* U^* \boldsymbol{f}$ per unit mass. The electrically conducting fluid of constant density ρ, kinematic viscosity ν, magnetic diffusivity η is permeated by an applied axisymmetric magnetic field $B^*\bar{\boldsymbol{b}}$. The magnetically insulating boundaries are located at radii $L^* r_i$ (inner) and $L^* r_o$ (outer); following H94, L^* is the shell gap width ($r_o - r_i := 1$) (see figure 1). Our detailed calculations are for the case of stress-free boundaries, though some of the implications for rigid boundaries will be noted.

We adopt L^*, U^* and B^* as our units of length, velocity and magnetic field. Our system is characterized by the Rossby, Ekman, magnetic Reynolds and Elsasser numbers

$$Ro := \frac{U^*}{L^*\Omega^*}, \qquad E := \frac{\nu}{L^{*2}\Omega^*}, \qquad Rm := \frac{L^* U^*}{\eta} \quad \text{and} \quad \Lambda := \frac{\sigma B^{*2}}{\rho \Omega^*}, \tag{1.1a–d}$$

where $\sigma = 1/\mu\eta$ is the electrical conductivity. We restrict attention to the slow flow limit

$$Ro \ll 1, \quad Rm \ll 1. \tag{1.2a,b}$$

Accordingly we write the total magnetic field in the form $\bar{\boldsymbol{b}} + Rm\boldsymbol{b}$. Linearization of the governing equations yields the system

$$2\hat{\boldsymbol{z}}\times\boldsymbol{u} = -\nabla p + \boldsymbol{f}_M + E\nabla^2\boldsymbol{u} + \boldsymbol{f} \quad (\nabla\cdot\boldsymbol{u} = 0), \tag{1.3a}$$

$$0 = \nabla\times\left(\boldsymbol{u}\times\bar{\boldsymbol{b}}\right) + \nabla^2\boldsymbol{b} \quad (\nabla\cdot\boldsymbol{b} = 0), \tag{1.3b}$$

where the 'hat' is used to denote unit vector,

$$\boldsymbol{f}_M = \Lambda[(\nabla\times\boldsymbol{b})\times\bar{\boldsymbol{b}} + (\nabla\times\bar{\boldsymbol{b}})\times\boldsymbol{b}] \tag{1.3c}$$

is the Lorentz force and p is the dimensionless pressure. It is helpful to regard the solution $\boldsymbol{b}$ of (1.3b) for given $\boldsymbol{u}$ subject to appropriate boundary conditions as a functional of $\boldsymbol{u}$. In turn (1.3c) determines $\boldsymbol{f}_M$ as a functional of $\boldsymbol{u}$ also:

$$\boldsymbol{f}_M[\boldsymbol{u}]. \tag{1.3d}$$

We adopt cylindrical polar coordinates (s, ϕ, z) and consider only applied body forces $\boldsymbol{f}$ that lead to flows with the symmetry

$$\left(u_s,\, u_\phi,\, u_z\right)(s, \phi, -z) = \left(u_s,\, u_\phi, -u_z\right)(s, \phi, z). \tag{1.4}$$

We limit our mathematical description to the Northern hemisphere with outer and inner boundaries $z = z_T(s)$ and $z = z_B(s)$ defined by

$$z_T := z_o \quad \text{and} \quad z_B := \begin{cases} z_i & \text{for } s < r_i \\ 0 & \text{for } s > r_i, \end{cases} \tag{1.5a}$$

where $z_o(s) = \sqrt{r_o^2 - s^2}$ and $z_i(s) = \sqrt{r_i^2 - s^2}$ define the z-coordinates of the outer and inner spheres. We denote their separation by

$$H(s) := z_T - z_B \quad \text{and introduce } H_i := H(r_i) \tag{1.5b}$$

https://doi.org/10.1017/S0022112099007776 Published online by Cambridge University Press

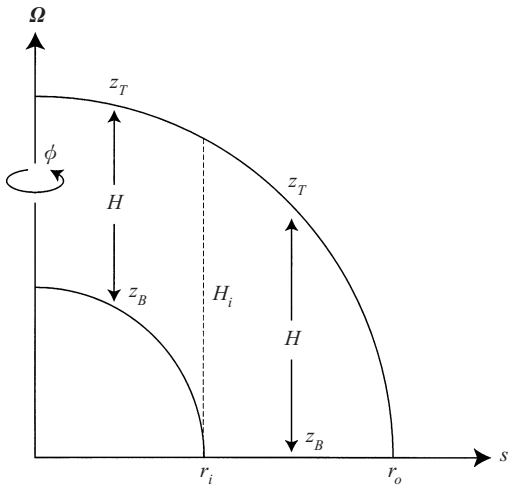


FIGURE 1. One quadrant of the shell geometry. The inner and outer spheres radii r_i and r_o respectively are shown together with the tangent cylinder height H_i identified by the broken line.

(see figure 1). On each boundary $z(s)$, we define normals

$$\boldsymbol{n} := \left(-\frac{\mathrm{d}z}{\mathrm{d}s}, 0, 1\right). \tag{1.5c}$$

For our spherical shell geometry they are

$$\boldsymbol{n}_T := \frac{\boldsymbol{r}}{z_T} \quad \text{and} \quad \boldsymbol{n}_B := \begin{cases} \boldsymbol{r}/z_B & \text{for } s < r_i \\ \widehat{\boldsymbol{z}} & \text{for } s > r_i, \end{cases} \tag{1.5d}$$

where $\boldsymbol{r} = (s, 0, z)$ is the radius vector. At the very least, our flow velocity satisfies the boundary condition

$$\boldsymbol{u} \cdot \boldsymbol{n} = 0 \quad \text{on both boundaries } z = z_T \text{ and } z_B. \tag{1.5e}$$

There are, of course, further conditions dependent on the nature of the boundaries, e.g. stress free or rigid, and electrically insulating or conducting.

Hollerbach & Proctor (1993) noted that, whereas generally (1.5*e*) is a single boundary condition, it becomes two at the equator of the inner sphere, where to avoid discontinuities the double condition

$$\widehat{\boldsymbol{z}} \cdot \boldsymbol{u} = \widehat{\boldsymbol{s}} \cdot \boldsymbol{u} = 0 \quad \text{at } s = r_i, z = 0 \tag{1.6}$$

must be met. On the basis of the boundary condition (1.5*e*) alone, they noted that an implication of the double condition (1.6) is

$$\mathscr{G}[\widehat{\boldsymbol{z}} \times \boldsymbol{u}] = 0 \tag{1.7a}$$

for solenoidal $\boldsymbol{u}$, where the functional $\mathscr{G}[\boldsymbol{F}]$, for some given vector field $\boldsymbol{F}$, is defined by

$$\mathscr{G}[\boldsymbol{F}] := \left[H_i \int_0^{H_i} \widehat{\boldsymbol{z}} \cdot (\nabla \times \boldsymbol{F}) \, \mathrm{d}z + r_i \int_0^{H_i} \widehat{\boldsymbol{s}} \cdot (\nabla \times \boldsymbol{F}) \, \mathrm{d}z \right]_{s=r_i} \tag{1.7b}$$

with $H_i = H(r_i)$. So upon application of $\mathscr{G}$ to the governing equation (1.3*a*), they

https://doi.org/10.1017/S0022112099007776 Published online by Cambridge University Press

showed that

$$\mathscr{A} := \mathscr{A}_M + \mathscr{A}_v + \mathscr{A}_f = 0, \tag{1.8a}$$

where

$$\mathscr{A}_f := \mathscr{G}[\boldsymbol{f}], \qquad \mathscr{A}_v := \mathscr{G}[E\nabla^2\boldsymbol{u}], \qquad \mathscr{A}_M := \mathscr{G}[\boldsymbol{f}_M]. \tag{1.8b}$$

In the absence of viscous and magnetic forces ($E = \Lambda = 0$), they pointed out that, for a given applied force $\boldsymbol{f}$, the integral $\mathscr{A} = \mathscr{A}_f$ is generally non-zero. By implication it is not possible to satisfy both conditions (1.6) simultaneously and as a result the flow exhibits a singularity on the tangent cylinder.

For finite values of the Ekman number ($E \neq 0$), the condition (1.6) and consequently (1.8a), namely $\mathscr{A} = 0$, is met by all physically realistic boundary conditions, so removing the singularity. For small E and in the absence of magnetic field ($\Lambda = 0$), however, large velocity gradients are expected to remain in shear layers on the tangent cylinder. This is confirmed by the numerical integrations reported both by Hollerbach & Proctor (1993) and H94. To investigate the extent to which the magnetic field can weaken the shear layers when $\Lambda \neq 0$, H94 considered the value of the ratio

$$\mathscr{Z} := \left| \frac{\mathscr{A}_f + \mathscr{A}_M}{\mathscr{A}_f} \right| = \left| \frac{\mathscr{A}_v}{\mathscr{A}_f} \right|. \tag{1.9}$$

As the identity shows, $\mathscr{Z}$ is really a measure of the size of the viscous force. Therefore its value depends on the character of the viscous layers and its evaluation provides a focal point for our boundary layer study. H94 found that $\mathscr{Z}$, at fixed E, is a decreasing function of Λ for the moderate values considered and so argued that the Lorentz force smooths out the discontinuity. Actually, the story is more complicated in the weak magnetic field limit

$$E \ll 1, \quad \Lambda \ll 1 \tag{1.10a,b}$$

to which we restrict analytic attention here and is also dependent on whether the applied magnetic field has dipole or quadrupole parity. We will, therefore, consider both the dipole field investigated by K-S, and the quadrupole field of H94.

1.3. *Summary of results*

Our paper is organized as follows. In § 2 we re-cap the main points of Hollerbach & Proctor's (1993) inviscid non-magnetic analysis $\Lambda = 0$ for which $\mathscr{Z} = 1$. That value gives the baseline about which the magnetic results $\Lambda \neq 0$ are judged.

The schematic figure 2 summarizes the radial extent of the various tangent cylinder boundary layers as a function of Λ. The pervading picture for all $\Lambda (\ll 1)$ is that of thick quasi-geostrophic layers, largely z-independent, which match to the external mainstream non-magnetic inhomogeneous geostrophic flow (2.1c) and contain inside them fully three-dimensional ageostrophic sublayers.

In § 3 we formulate the quasi-geostrophic boundary layer equations which, due to the asymmetric nature of the flow, differ significantly from those considered by K-S for the axisymmetric case. Specifically, they are fourth- rather than second-order ordinary differential equations, which generally reveal a double layer structure. Nevertheless, for $\Lambda \ll E^{1/2}\,(E^{3/7})$, the layer on the exterior *equatorial* § 4.1 (interior *polar* § 4.2) side continues to be simply a magnetotopographic variant of the viscous $E^{1/4}\,(E^{2/7})$-Stewartson layer. When $\Lambda \gg E^{1/2}\,(E^{3/7})$ the layer splits into a thicker inviscid $\Lambda^{1/2}\,(\Lambda^{2/3})$-magnetotopographic layer for $\Lambda \ll 1$ and a thinner viscous $(E/\Lambda)^{1/2}$-Hartmann layer for $\Lambda \ll E^{1/3}$. Though the Lorentz force in the magnetotopographic

https://doi.org/10.1017/S0022112099007776 Published online by Cambridge University Press

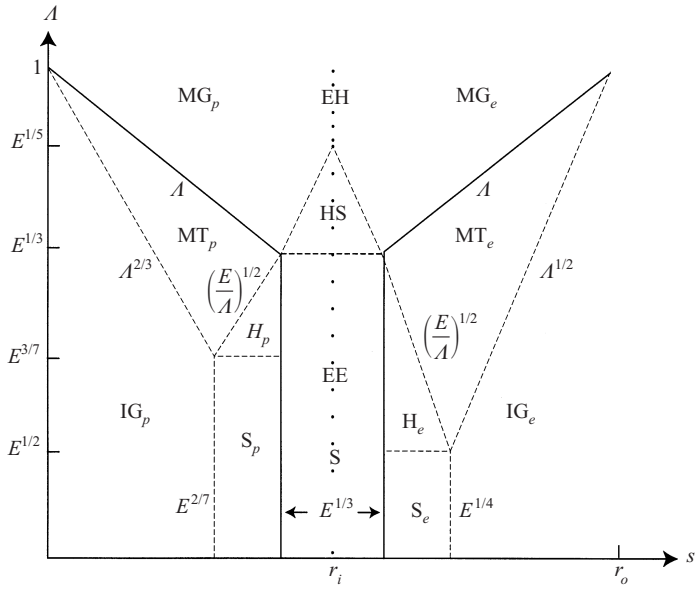


FIGURE 2. A schematic diagram locating the radial s-extent of the tangent-cylinder shear layers for various values of Λ in the case of magnetic fields with quadrupole parity. The quasi-geostrophic domains of the $E^{1/4}$, $E^{2/7}$-Stewartson (S), the $(E/\Lambda)^{1/2}$-Hartmann (H) and the $\Lambda^{1/2}$, $\Lambda^{2/3}$-magnetotopographic (MT) layers all lie outside the continuous lines but are bounded at their extremities by the mainstream inhomogeneous geostrophic (IG) flow domains. Inside lie the ageostrophic domains of the $E^{1/3}$-Stewartson (S), the Hartmann–Stewartson stump (HS) and the Λ-magnetogeostrophic (MG) layers. *Equatorial* and *polar* domains are distinguished by the subscripts e and p and their boundaries are marked by broken lines. The existence of $E^{2/5}$-equatorial Ekman (EE) and the $(E/\Lambda)^{1/2}$-equatorial Hartmann (EH) layers is marked by the large and small dots respectively along the line $s = r_i$.

layers partially smooths out the shear structure, considerable shear gradients remain in the viscous sublayers which are exacerbated by the shortenning Hartmann length scale. Consequently, the solutions obtained in § 4 show, contrary to the suggestion by H94, that $\mathscr{Z}$ is an increasing function of Λ throughout the range $\Lambda \ll E^{1/3}$ (see (4.8) and (4.37)).

In § 5.1 the ageostrophic sublayer problem is formulated. It is noted that non-axisymmetric effects are unimportant and so motion is governed, as in K-S, by equations (5.4). When $\Lambda = E^{1/3}$, the quasi-geostrophic Hartmann-layer merges with the $E^{1/3}$-Stewartson layer. For larger values of Λ, the ageostrophic layer splits into two. On the one hand, the outer inviscid Λ-magnetogeostrophic layer § 5.2.1 thickens and matches externally with the magnetotopographic layer, as exemplified by the formulation (5.3). On the other, the thinning viscous Hartmann–Stewartson layer § 5.2.2 detaches itself from the outer sphere boundary forming a shrinking stump attached to the equator of the inner sphere. Since the size of the stump is sensitive to the magnitude of the radial magnetic field near the equator, there are significant differences between dipole and quadrupole parity fields. Very large shear gradients are maintained in the stump causing $\mathscr{Z}$ to continue to increase. For dipole parity, the stump persists throughout the range $E^{1/3} \ll \Lambda \ll 1$ with the corresponding increasing value of $\mathscr{Z}$ for model K-S being given by (5.28).

The ageostrophic flow in the vicinity of the inner-sphere equator for model H94 with quadrupole parity is discussed in § 6. Analytic progress is possible through the

https://doi.org/10.1017/S0022112099007776 Published online by Cambridge University Press

construction of a new magnetogeostrophic solution in § 6.1 to which internal viscous boundary layers § 6.2 are matched. As Λ increases from $O(E^{1/3})$, the most significant feature is the collapse of the $(E/\Lambda)^{1/2}$-Hartmann–Stewartson layer stump into the $E^{2/5}$-equatorial Ekman layer, which occurs when $\Lambda = O(E^{1/5})$ (see § 6.2.2 and figure 4 below) marking the maximum of $\mathscr{Z}$ as given by (5.27) in the range $E^{1/3} \ll \Lambda \ll E^{1/5}$. When $E^{1/5} \ll \Lambda \ll 1$ the equatorial layer continues to thin and takes on the form of a Hartmann layer which spreads in concert poleward about the inner sphere (see figure 5 below). Its strength is dependent on the boundary conditions and is particularly weak for the stress-free boundary adopted by H94. This layer provides the sole contribution to $\mathscr{Z}$ which now decreases with increasing Λ. The analytic solution (6.8), (6.12) presented in § 6.2.1 shows that $\mathscr{Z} = O(1)$ when $\Lambda = O(E^{3/25})$ (see (6.19)) and thereafter is small.

We are also careful, where possible, with our order of magnitude error estimates. They indicate that extreme values of the parameters are required to enter the asymptotic regimes. Nevertheless, even with the relatively moderate values employed for the numerics, the results illustrated in figure 6 below support the trends predicted by the asymptotics. We should stress that our emphasis on the value of $\mathscr{Z}$ is not because of its physical context, which is obscure. Rather it is a diagnostic which provides a succinct measure of viscous shear on the tangent cylinder. We use it to test the applicability of our boundary layer theory to the results of numerical experiment.

2. Inviscid non-magnetic limit

When $E = \Lambda = 0$, we may write the solution in the form

$$\boldsymbol{u} = \boldsymbol{u}_f(s, \phi, z) + \boldsymbol{U}_G(s, \phi), \tag{2.1a}$$

where $\boldsymbol{u}_f(s, \phi, z)$ is a particular integral of

$$2\widehat{\boldsymbol{z}} \times \boldsymbol{u}_f = -\nabla p_f + \boldsymbol{f} \quad (\nabla \cdot \boldsymbol{u}_f = 0) \tag{2.1b}$$

and

$$\boldsymbol{U}_G(s, \phi) = \left(\frac{1}{s} \frac{\partial \Phi_G}{\partial \phi}, -\frac{\partial \Phi_G}{\partial s}, W_G \right) \tag{2.1c}$$

is the appropriate additional geostrophic flow (pressure $P_G = -2\Phi_G$) required to meet the vanishing of the normal velocity on the inner and outer spherical boundaries.

For a specific model problem, we consider a single azimuthal harmonic and set

$$(\boldsymbol{u}, p, \boldsymbol{f}) = \mathrm{Re}\,[(\boldsymbol{u}^\dagger, p^\dagger, \boldsymbol{f}^\dagger)\, \mathrm{e}^{\mathrm{i}m\phi}]. \tag{2.2}$$

In view of the linearity, this is the only harmonic involved. So henceforth we use this complex notation and for clarity drop the superscript †. We generalize the $m = 1$ example of H94 to

$$\boldsymbol{u}_f = \left(-\frac{\mathrm{i}m}{\gamma + 1} \frac{s^{m-1} z^2}{r_i^m H_i^2}, \frac{s^{m-1}(\gamma s^2 + m z^2)}{(\gamma + 1) r_i^m H_i^2}, -\frac{\mathrm{i}m\gamma}{\gamma + 1} \frac{s^m z}{r_i^m H_i^2} \right), \tag{2.3a}$$

$$p_f = \frac{2}{\gamma + 1} \frac{s^m z^2}{r_i^m H_i^2}, \qquad \boldsymbol{f} = \left(-\frac{2\gamma}{\gamma + 1} \frac{s^{m+1}}{r_i^m H_i^2}, 0, \frac{4}{\gamma + 1} \frac{s^m z}{r_i^m H_i^2} \right), \tag{2.3b}$$

where γ is an arbitrary constant. It is included to stress the wide range of applicability of the model. Indeed, the special case $\gamma = -2$ is particularly pertinent, as it corresponds to the body force on a particular density distribution in a radial gravitational field.

https://doi.org/10.1017/S0022112099007776 Published online by Cambridge University Press

Since the the radial component of the velocity (2.3*a*) is given by

$$\boldsymbol{r}\cdot\boldsymbol{u}_f = -\mathrm{i}m\frac{s^m z^2}{r_i^m H_i^2}, \tag{2.4a}$$

direct integration of (2.1*b*) yields

$$\mathscr{A}_f = 2\mathscr{G}[\widehat{\boldsymbol{z}}\times\boldsymbol{u}_f] = -2\,\boldsymbol{r}\cdot\boldsymbol{u}_f\big|_{r=(r_i,H_i)} = 2\mathrm{i}m. \tag{2.4b}$$

In view of the fact that $\boldsymbol{r}\cdot\boldsymbol{u}_f$ does not vanish on either the inner or outer spheres except on the equator $z = 0$, the geostrophic flow necessary to meet the boundary condition (1.5*e*) is given by

$$\Phi_G = \begin{cases} -\dfrac{s^m z_o z_i}{r_i^m H_i^2} & \text{in IG}_p \quad s < r_i \\ \dfrac{s^m z_o^2}{r_i^m H_i^2} & \text{in IG}_e \quad s > r_i, \end{cases} \tag{2.5a}$$

$$W_G = \begin{cases} \mathrm{i}m\dfrac{s^m(z_o + z_i)}{r_i^m H_i^2} & \text{in IG}_p \quad s < r_i \\ 0 & \text{in IG}_e \quad s > r_i, \end{cases} \tag{2.5b}$$

where here and below the domain labelling is that introduced on figure 2.

As noted by Hollerbach & Proctor (1993) for their case $m = \gamma = 1$, there is a flow discontinuity on the tangent cylinder $s = r_i$. Its most important manifestation is the discontinuity of the radial velocity $\mathrm{i}m\Phi_G/s$. It implies the existence of an azimuthal jet on the tangent cylinder in order to accommodate mass flux continuity. It must be stressed that this feature is generic and will only be absent for very special choices of the body force. When small viscous and Lorentz forces are introduced the flow continues to be given by (2.1), (2.3) and (2.5) in the mainstream outside boundary layers. Our objective is to investigate how the discontinuity exhibited by (2.5) is resolved with the additional small forces.

3. Quasi-geostrophic flow regime

When the Ekman and Elsasser numbers are small, the corrections to the flow $\boldsymbol{u} = \boldsymbol{u}_f + \boldsymbol{U}_G$ obtained above are small in the mainstream outside Ekman–Hartmann boundary layers adjacent to the inner and outer spherical boundaries $r = r_i$ and r_o as well as the tangent-cylinder shear layer $s = r_i$. To resolve the nature of the latter, we are guided by the results of K-S, which suggest that the main adjustments in the shear layer are quasi-geostrophic provided that

$$\Lambda \ll E^{1/3}; \tag{3.1}$$

we will focus attention on this limit throughout this section. We will also assume that the shear layer width $\delta_{sl}L^*$ (say) is small compared to the azimuthal length scale:

$$m\delta_{sl} \ll 1. \tag{3.2}$$

At this stage it is inappropriate to specify the value of δ_{sl}, which is a complicated function of m, Λ and E and possibly multi-valued to accommodate multiple layers.

Restricting attention to the harmonic (2.2), we continue with the complex representation and describe the flow outside any Ekman–Hartmann layers adjacent to the

https://doi.org/10.1017/S0022112099007776 Published online by Cambridge University Press

inner and outer spheres by

$$\boldsymbol{u} = \boldsymbol{u}_f + \widetilde{\boldsymbol{u}}, \quad p = p_f + \widetilde{p}. \tag{3.3}$$

The additional terms $\widetilde{\boldsymbol{u}}$ and $\widetilde{p}$ are close to $\boldsymbol{U}_G$ and P_G in the mainstream outside the tangent-cylinder shear layer but differ significantly from them in it. Nevertheless, even in the shear layer, motion remains quasi-geostrophic and so it is helpful to take z-averages

$$\langle \cdots \rangle := \frac{1}{H}\int_{z_B}^{z_T} \cdots \, \mathrm{d}z \tag{3.4}$$

of the governing equations. In so doing, we rely heavily on the existence of large radial shears in the quasi-geostrophic flow and make approximations on the basis of the short radial length scale limit (3.2). It means that, in solving the governing equation (1.3) for $\widetilde{\boldsymbol{u}}$ and $\widetilde{p}$, we ignore the ageostrophic flow forced by the inhomogeneous viscous ($E\nabla^2\boldsymbol{u}_f$) and magnetic ($\boldsymbol{f}_M[\boldsymbol{u}_f]$, see (1.3$d$)) terms, as well as curvature effects; both are linked to variations on an $O(1)$ radial length scale. We largely, but not always, ignore the radial derivative of H and ϕ-derivatives of other quantities. These are sensitive matters, which are crucial to our quasi-geostrophic approximations, which we apply with care.

On the basis of the above approximations the radial (s) and azimuthal (ϕ) components of the z-averaged equation (1.3a) are approximately

$$-2\langle \widetilde{u}_\phi \rangle = -\frac{\mathrm{d}\langle \widetilde{p} \rangle}{\mathrm{d}s}, \tag{3.5a}$$

$$2\langle \widetilde{u}_s \rangle = -\frac{\mathrm{i}m\langle \widetilde{p} \rangle}{s} - \Lambda_i \langle \widetilde{u}_\phi \rangle + E\frac{\mathrm{d}^2\langle \widetilde{u}_\phi \rangle}{\mathrm{d}s^2}, \tag{3.5b}$$

where

$$\Lambda_i = \Lambda \langle \overline{b}_s^2 \rangle_{s=r_i}. \tag{3.5c}$$

The essential idea is that the motion is almost geostrophic and so we have only retained the largest of the other terms, which are yet small compared to the basic geostrophic balance. The nature of the approximation is first clarified by considering the axisymmetric $m = 0$ case investigated by K-S. They essentially derived (3.5b) and followed Taylor's (1963) recipe of considering mass flux in and out of cylinders as a means of fixing the magnitude of the degenerate quasi-geostrophic flow $\langle \widetilde{u}_\phi \rangle$. That argument now has to be modified because of the ϕ-component of the pressure gradient in (3.5b). Nevertheless, the spirit of Taylor's argument persists provided m is not too large, in the sense of (3.2).

The geometry has important implications for mass conservation ($\nabla \cdot \widetilde{\boldsymbol{u}} = 0$); it implies that

$$\nabla \cdot \left(H\langle \widetilde{\boldsymbol{u}} \rangle \right) = -\widetilde{\boldsymbol{u}}_T \cdot \boldsymbol{n}_T + \widetilde{\boldsymbol{u}}_B \cdot \boldsymbol{n}_B. \tag{3.6}$$

So multiplying each component of (3.5a, b) by H and taking the divergence of $H\langle \widetilde{\boldsymbol{u}} \rangle$ yields

$$E\frac{\mathrm{d}^3\langle \widetilde{u}_\phi \rangle}{\mathrm{d}s^3} - \Lambda_i \frac{\mathrm{d}\langle \widetilde{u}_\phi \rangle}{\mathrm{d}s} - \frac{\mathrm{i}m\langle \widetilde{p} \rangle}{r_i H_i}\frac{\mathrm{d}H}{\mathrm{d}s} = -\frac{2}{H_i}\left[\widetilde{\boldsymbol{u}}_T \cdot \boldsymbol{n}_T - \widetilde{\boldsymbol{u}}_B \cdot \boldsymbol{n}_B\right]. \tag{3.7}$$

Here we have again ignored curvature effects and variations in height H except where it leads to the topographic term proportional to $\mathrm{i}m\langle \widetilde{p} \rangle$. This term was absent in the axisymmetric analysis of K-S; here it is crucial and corresponds to the vortex line stretching term usually associated with topographic Rossby waves.

https://doi.org/10.1017/S0022112099007776 Published online by Cambridge University Press

Like Taylor's (1963) condition for axisymmetric flows and modified versions of it, (3.7) is a consistency condition necessary for removing the geostrophic degeneracy present in (3.5*a*), which is resolved by the terms of smaller order in (3.5*b*). So at leading order the solution is

$$\langle \widetilde{\boldsymbol{u}} \rangle = \boldsymbol{U} + \text{smaller terms}, \quad \langle \widetilde{p} \rangle = P + \text{smaller terms}, \tag{3.8a}$$

where the dominant geostrophic contribution is

$$\boldsymbol{U}(s,\phi) := \left(\frac{\mathrm{i}m\Phi}{s}, -\frac{\partial \Phi}{\partial s}, W \right), \qquad P = -2\Phi. \tag{3.8b}$$

Thus Φ is determined at lower order by the consistency condition (3.7) (see (3.12) below). Importantly, $\boldsymbol{U}$ merges with the geostrophic flow $\boldsymbol{U}_G$ defined by (2.1*c*) and (2.4) on leaving the shear layer:

$$\Phi - \Phi_G \to 0 \quad \text{and} \quad W - W_G \to 0 \quad \text{as } |(s - r_i)/\delta_{sl}| \to \infty. \tag{3.9}$$

To complete the formulation of the shear layer problem, we need to apply the normal fluid flux boundary condition at the edge of the Ekman layers adjacent to the inner and outer spheres, namely

$$\widetilde{\boldsymbol{u}} \cdot \boldsymbol{n} = -\boldsymbol{u}_f \cdot \boldsymbol{n} + \text{Ekman flux contribution}, \tag{3.10a}$$

depending on whether the boundaries are rigid or stress free. From this the dominant contribution to the right-hand side of (3.7) is

$$\boldsymbol{u}_{fT} \cdot \boldsymbol{n}_T - \boldsymbol{u}_{fB} \cdot \boldsymbol{n}_B = -\mathrm{i}\, m \frac{s^m H}{r_i^m H_i^2} \quad (0 \leqslant s \leqslant r_o). \tag{3.10b}$$

Finally, the topographic term requires the asymptotic value

$$\frac{\mathrm{d}H}{\mathrm{d}s} + \frac{r_i}{H_i} \sim \begin{cases} \sqrt{\dfrac{r_i}{-2x}} & \text{for } x < 0 \\ 0 & \text{for } x > 0 \end{cases} \tag{3.11a}$$

valid for small $|x| = O(\delta_{sl})$, where we have introduced the local radial coordinate

$$x = s - r_i. \tag{3.11b}$$

Substitution of the above results into (3.7) leads to the equations

$$E \frac{\mathrm{d}^4 \Phi}{\mathrm{d}x^4} - E^{1/2} \frac{\mathrm{d}}{\mathrm{d}x} \left(\sigma \frac{\mathrm{d}\Phi}{\mathrm{d}x} \right) - \Lambda_i \frac{\mathrm{d}^2 \Phi}{\mathrm{d}x^2} = \begin{cases} \dfrac{2\mathrm{i}m}{H_i^2} \left[\left(\dfrac{H_i}{\sqrt{-2r_i x}} - 1 \right) \Phi + 1 \right] & \text{for } x < 0 \\ \dfrac{2\mathrm{i}m}{H_i^2} (-\Phi + 1) & \text{for } x > 0, \end{cases} \tag{3.12a}$$

where for
(i) stress-free boundaries

$$\sigma = 0; \tag{3.12b}$$

https://doi.org/10.1017/S0022112099007776 Published online by Cambridge University Press

(ii) rigid boundaries

$$\sigma - \frac{1}{H_i}\left(\frac{r_o}{H_i}\right)^{1/2} = \begin{cases} \dfrac{1}{H_i}\left(\dfrac{r_i}{-2x}\right)^{1/4} & \text{for } x < 0 \\ 0 & \text{for } x > 0, \end{cases} \tag{3.12c}$$

as shown, for example, by K-S equations (3.4*b*) and (3.9).

Equation (3.12*a*) must be solved subject to

$$\Phi \to \begin{cases} -\dfrac{\sqrt{-2r_i x}}{H_i} & \text{as } x/\delta_{sl} \downarrow -\infty \\ 1 & \text{as } x/\delta_{sl} \uparrow \infty, \end{cases} \tag{3.13a}$$

while at the tangent cylinder we require

$$\text{continuity of} \quad \Phi, \quad \frac{\mathrm{d}\Phi}{\mathrm{d}x}, \quad \frac{\mathrm{d}^2\Phi}{\mathrm{d}x^2}, \quad \frac{\mathrm{d}^3\Phi}{\mathrm{d}x^3} - \frac{\sigma}{E^{1/2}}\frac{\mathrm{d}\Phi}{\mathrm{d}x} \quad \text{across } x = 0. \tag{3.13b}$$

Using the magnitude of the Lorentz force calculated, we see that

$$\mathscr{A}_M = H_i^2 \Lambda_i \left.\frac{\mathrm{d}^2\Phi}{\mathrm{d}x^2}\right|_{x=0}, \tag{3.14a}$$

which together with (2.3*d*) gives

$$\mathscr{Z} = \left|1 - \mathrm{i}\,\delta_{\Lambda e}^2 \left.\frac{\mathrm{d}^2\Phi}{\mathrm{d}x^2}\right|_{x=0}\right| \qquad \left(\delta_{\Lambda e} := \sqrt{\frac{H_i^2\Lambda_i}{2m}}\right). \tag{3.14b}$$

In the next section we solve the boundary layer equations (3.12*a*) and calculate $\mathscr{Z}$.

4. Shear layer structure

We need to solve (3.12) for positive and negative x separately and then apply continuity conditions across $x = 0$. The asymptotics involves two pairs of parameters Δ_E, ε_E and Δ_Λ, ε_Λ generated from the two independent small numbers E and Λ. We introduce them in the text, when required. Nevertheless, some error estimates involve them prior to their introduction and so we find it convenient to list them together with all the key lengths in Appendix A. In order not to proliferate more than necessary the number of parameter ranges, we assume that

$$m = O(1). \tag{4.1}$$

4.1. *Exterior layers*

The solution of (3.12) on the *equatorial* side $x > 0$ of the tangent cylinder, which satisfies $\Phi \to 0$ as $x \uparrow \infty$, is

$$\Phi = 1 - \frac{\lambda_+(1+\alpha_-)\mathrm{e}^{-\lambda_- x} - \lambda_-(1+\alpha_+)\mathrm{e}^{-\lambda_+ x}}{\lambda_+ - \lambda_-}. \tag{4.2a}$$

Here the constants $\alpha_\pm$ are fixed by the $x = 0$ values of Φ and its derivative:

$$\alpha_\pm = \left[-\frac{1}{\lambda_\mp}\frac{\mathrm{d}\Phi}{\mathrm{d}x} - \Phi\right]_{x=0}. \tag{4.2b}$$

https://doi.org/10.1017/S0022112099007776 Published online by Cambridge University Press

The values of λ_- ($\pi/4 \leqslant \arg\lambda_- \leqslant 3\pi/8$) and λ_+ ($-\pi/8 \leqslant \arg\lambda_+ \leqslant 0$) are given by

$$\lambda_\pm^2 := \frac{1}{2}\left(\frac{1}{\delta_H^2} + \frac{\sigma_o}{\delta_{Ee}^2}\right) \pm \left[\frac{1}{4}\left(\frac{1}{\delta_H^2} + \frac{\sigma_o}{\delta_{Ee}^2}\right)^2 - \frac{\mathrm{i}}{\delta_{Ee}^4}\right]^{1/2} \tag{4.3a}$$

(see (4.4)), where significantly the product

$$\lambda_+\lambda_- = \frac{\mathrm{e}^{\mathrm{i}\pi/4}}{\delta_{Ee}^2} \tag{4.3b}$$

is independent of both Λ and

$$\sigma_o = \begin{cases} 0 & \text{stress-free} \\ \left(\dfrac{r_o}{2mH_i}\right)^{1/2} & \text{rigid.} \end{cases} \tag{4.4a}$$

The viscous and magnetic length scales relevant to the form of $\lambda_\pm$ are

$$\delta_{Ee} := \left(\frac{EH_i}{m}\right)^{1/4}\left(\frac{H_i}{2}\right)^{1/4}, \qquad \delta_{\Lambda e} := \left(\frac{\Lambda_i H_i}{m}\right)^{1/2}\left(\frac{H_i}{2}\right)^{1/2}, \tag{4.4b}$$

which together define the Hartmann length

$$\delta_H := \left(\frac{E}{\Lambda_i}\right)^{1/2} \quad \text{with } \delta_{\Lambda e}\delta_H = \delta_{Ee}^2. \tag{4.4c}$$

We can identify two asymptotic regimes. In one case, the boundary layer S_e has a single viscous length scale δ_{Ee}:

$$\lambda_\pm = O\left(\frac{1}{\delta_{Ee}}\right) \quad \text{for } \Lambda \leqslant O\left((mE)^{1/2}\right). \tag{4.5}$$

In the other, it has a double layer structure:

$$\lambda_- \approx \frac{\mathrm{e}^{\mathrm{i}\pi/4}}{\delta_{\Lambda e}}, \quad \lambda_+ \approx \frac{1}{\delta_H} \quad \text{for } \Lambda \gg (mE)^{1/2}. \tag{4.6a}$$

Here λ_+ identifies the thin Hartmann layer H_e of width $O(\delta_H)$, while λ_- corresponds to a thicker magnetotopographic layer MT_e of thickness $O(\delta_{\Lambda e})$:

$$\delta_H \ll \delta_{Ee} \ll \delta_{\Lambda e} \quad \text{for } \Lambda \gg (mE)^{1/2}. \tag{4.6b}$$

From a general point of view the longest boundary length on the *equatorial* side always exceeds that on the *polar* side ($x < 0$). As a consequence, the main role of the exterior layer is to bring Φ close to zero on the tangent cylinder $x = 0$. This reduces as much as possible the singularity of $\Phi/\sqrt{-x}$ in (3.12*a*) as $x \uparrow 0$. Furthermore, in the viscous regime on the equatorial side ($\Lambda \ll E^{3/7}$, identified in §4.2.1 below), we find that the derivative $\mathrm{d}\Phi/\mathrm{d}x$ also vanishes at the origin at lowest order. More precisely, the result (4.15) below shows that both α_+ and α_- are small, which in turn establishes with use of (4.2) the smallness of Φ and $\mathrm{d}\Phi/\mathrm{d}x$ at $x = 0$. Within the framework of the approximation ($\alpha_\pm \approx 0$), (4.2*a*) gives

$$\left.\frac{\mathrm{d}^2\Phi}{\mathrm{d}x^2}\right|_{x=0} \approx \frac{\mathrm{e}^{\mathrm{i}\pi/4}}{\delta_{Ee}^2} = \frac{\mathrm{e}^{\mathrm{i}\pi/4}}{\delta_{\Lambda e}\delta_H} \quad \text{for } \Lambda \ll m^{4/7}E^{3/7}, \tag{4.7}$$

independent of both Λ and σ_o because of the property (4.3*b*). The lack of dependence

https://doi.org/10.1017/S0022112099007776 Published online by Cambridge University Press

on σ is particularly interesting because it indicates that the result is independent of whether the boundary is rigid or stress-free. Since this second derivative is continuous across $x = 0$, we conclude that (3.14b) yields

$$\mathscr{Z} = \left| 1 + \mathrm{e}^{-\mathrm{i}\pi/4}\, \frac{\delta_{\Lambda e}}{\delta_H}\, (1 + O(\Upsilon)) \right| \quad \text{for } \Lambda \ll m^{4/7} E^{3/7}, \tag{4.8a}$$

where the error estimate $O(\Upsilon)$ (see (4.13a) below) is established by (4.18) below. At fixed E, (4.8a) indicates that $\mathscr{Z}$ is an increasing function of Λ:

$$\mathscr{Z} = \begin{cases} O(1) & \text{for } \Lambda \leqslant O\left((mE)^{1/2}\right) \\ O\left(\dfrac{\Lambda}{(mE)^{1/2}}\right) & \text{for } (mE)^{1/2} \ll \Lambda \ll m^{4/7} E^{3/7}. \end{cases} \tag{4.8b}$$

4.2. *Interior layers*

The boundary conditions on the solution of (3.12a) in the interior layer on the *polar* side $x < 0$ of the tangent cylinder are determined by the continuity conditions (3.13b) and the exterior solution (4.2a). They give

$$\frac{\mathrm{d}^2\Phi}{\mathrm{d}x^2} + (\lambda_+ + \lambda_-)\, \frac{\mathrm{d}\Phi}{\mathrm{d}x} + \lambda_+\lambda_-(\Phi - 1) = 0, \tag{4.9a}$$

$$\left[\frac{\mathrm{d}^3\Phi}{\mathrm{d}x^3} - \frac{\sigma}{E^{1/2}}\, \frac{\mathrm{d}\Phi}{\mathrm{d}x} \right]_{x\uparrow 0} + (\lambda_+ + \lambda_-)\, \frac{\mathrm{d}^2\Phi}{\mathrm{d}x^2} + \left(\left[\frac{\sigma}{E^{1/2}} \right]_{x\downarrow 0} + \lambda_+\lambda_- \right) \frac{\mathrm{d}\Phi}{\mathrm{d}x} = 0 \tag{4.9b}$$

at $x = 0$. The nature of the solution depends on the relative sizes of Λ and E. The key viscous and magnetic lengths are

$$\delta_{Ep} := \left(\frac{E H_i}{m} \right)^{2/7} \left(\frac{r_i}{2} \right)^{1/7}, \qquad \delta_{\Lambda p} := \left(\frac{\Lambda_i H_i}{m} \right)^{2/3} \left(\frac{r_i}{2} \right)^{1/3}; \tag{4.10a}$$

they are linked to the Hartmann length δ_H by

$$\delta_{\Lambda p}^3 \delta_H^4 = \delta_{Ep}^7. \tag{4.10b}$$

There are two main parameter ranges identified by the magnitude of the ratio

$$\Delta_E := \frac{\delta_{Ep}}{\delta_H} = \left(\frac{\Lambda_i}{E^{3/7}} \right)^{1/2} \left(\frac{r_i H_i^2}{2m^2} \right)^{1/7}, \tag{4.11}$$

which we investigate separately.

4.2.1. *Viscous regime* ($\varepsilon_\Lambda \ll \varepsilon_E^2$)

In the small-Δ_E parameter range

$$\Lambda \ll m^{4/7} E^{3/7} \quad (\Delta_E \ll 1) \tag{4.12}$$

(equivalently $\varepsilon_\Lambda \ll \varepsilon_E^2$; see (A 2$b$)), the Lorentz force is unimportant and the resulting viscous layer S_p has the single length scale δ_{Ep}. Of importance in the application of the boundary conditions (4.9) at the tangent cylinder $x = 0$ is its ratio to the shortest length scale $|\lambda_+^{-1}|$ in the exterior layer:

$$\Upsilon := |\lambda_+ \delta_{Ep}| = \begin{cases} O(\varepsilon_E) & \text{for } \Lambda \leqslant O\left((mE)^{1/2}\right) \\ O(\Delta_E) & \text{for } (mE)^{1/2} \ll \Lambda \ll m^{4/7} E^{3/7}, \end{cases} \tag{4.13a}$$

https://doi.org/10.1017/S0022112099007776 Published online by Cambridge University Press

where

$$\varepsilon_E := \frac{\delta_{Ep}}{\delta_{Ee}} = \left(\frac{EH_i}{m}\right)^{1/28} \left(\frac{r_i}{2}\right)^{1/7} \left(\frac{2}{H_i}\right)^{1/4} (\ll 1). \tag{4.13b}$$

Since the interior viscous length scale δ_{Ep} is shorter than any of the length scales of the exterior boundary layer, most of the required adjustment of Φ occurs in the exterior layer, while the main adjustments to the higher derivatives, which dominate (4.9), occur in the interior layer. The crucial balance on the tangent cylinder in (4.9*a*) is dominated by $\mathrm{d}^2\Phi/\mathrm{d}x^2 \approx \lambda_+\lambda_-$, consistent with (4.7) above. In turn, it sets the scale for the small interior solution:

$$\Phi = \varepsilon_E^2 \Phi_p(\xi) \quad \text{with } \xi = x/\delta_{Ep}. \tag{4.14}$$

Together with (4.2*b*) and (4.3*b*) we obtain the explicit expressions

$$\alpha_\pm = -\mathrm{e}^{-\mathrm{i}\pi/4}\, \lambda_\pm \delta_{Ep} \frac{\mathrm{d}\Phi_p}{\mathrm{d}\xi}(0) - \varepsilon_E^2 \Phi_p(0) = O(\Upsilon) \tag{4.15}$$

for the coefficients of the exterior solution (4.2*a*). Here the error estimate comes from the size of the coefficient of the first derivative. The necessary smallness of $\alpha_\pm$ confirms our limitation to the range (4.12).

As pointed out in § 4.1, the lowest-order result (4.15) is sufficient to establish (4.7) and the value (4.8) of the measure $\mathscr{Y}$. Nevertheless for completeness, we outline the problem for Φ_p and indicate how the expansion can proceed consistently. According to (3.12*a*), Φ_p satisfies

$$\frac{\mathrm{d}^4\Phi_p}{\mathrm{d}\xi^4} - \frac{\mathrm{d}}{\mathrm{d}\xi}\left[\left(\frac{\sigma_i}{(-\xi)^{1/4}} + \Delta_E^2\right)\frac{\mathrm{d}\Phi_p}{\mathrm{d}\xi}\right] - \mathrm{i}\left(\frac{1}{\sqrt{-\xi}} - \varepsilon_E^4\right)\Phi_p = \mathrm{i}\varepsilon_E^2, \tag{4.16a}$$

where

$$\sigma_i = \begin{cases} 0 & \text{stress-free} \\ \left(\dfrac{r_i}{2mH_i}\right)^{1/2} & \text{rigid.} \end{cases} \tag{4.16b}$$

Throughout the small-Δ_E range (4.12), the boundary conditions (4.9) reduce to

$$\frac{\mathrm{d}^2\Phi_p}{\mathrm{d}\xi^2} = \frac{1+\mathrm{i}}{\sqrt{2}} + O(\Upsilon), \quad \left.\begin{aligned} \frac{\mathrm{d}^3\Phi_p}{\mathrm{d}\xi^3} - \sigma_i \frac{\mathrm{d}\Phi_p}{\mathrm{d}\xi} &= O(\Upsilon) \quad \text{at } \xi = 0, \\ \Phi_p &\to 0 \quad \text{as } \xi \to \infty. \end{aligned}\right\} \tag{4.17}$$

The lowest-order problem involves solving (4.16*a*) with the terms proportional to Δ_E^2 and ε_E^2 neglected subject to the boundary conditions (4.17). The way that we approximate the boundary conditions again emphasizes the limitation of the validity of our solution to small Υ.

Finally, we note that, with the solution of (4.16) and (4.17), we may obtain the exact representation

$$\left.\frac{\mathrm{d}^2\Phi}{\mathrm{d}x^2}\right|_{x=0} = \frac{1}{\delta_{Ee}^2}\left[\mathrm{e}^{\mathrm{i}\pi/4}\left(1 - \varepsilon_E^2\Phi_p(0)\right) - \delta_{Ep}\left(\lambda_+ + \lambda_-\right)\frac{\mathrm{d}\Phi_p}{\mathrm{d}\xi}(0)\right], \tag{4.18}$$

in which the coefficient of the first derivative $\mathrm{d}\Phi_p/\mathrm{d}\xi(0)$ is $O(\Upsilon)$. In this way the solution of (4.16) and (4.17) determines the $O(\Upsilon)$ corrections to (4.7). Accordingly,

https://doi.org/10.1017/S0022112099007776 Published online by Cambridge University Press

(4.8*a*) yields

$$\mathscr{Y} = \begin{cases} \left[1 + \sqrt{2}\,\dfrac{\delta_{\Lambda e}}{\delta_H} + \left(\dfrac{\delta_{\Lambda e}}{\delta_H}\right)^2\right]^{1/2} + O(\varepsilon_E) & \text{for } \Lambda \leqslant O((mE)^{1/2}) \\ \dfrac{\delta_{\Lambda e}}{\delta_H}\,(1 + O(\Delta_E)) & \text{for } (mE)^{1/2} \ll \Lambda \ll m^{4/7}E^{3/7}. \end{cases} \tag{4.19}$$

When $\Delta_E = O(1)$, the scaling (4.14) of Φ remains valid, but we must now solve (4.16) subject to (4.9) without its simplification to (4.17). Its solution is essential, however, to determine $\mathrm{d}\Phi_p/\mathrm{d}\xi(0)$, which makes a leading-order contribution to the exact expression (4.18). This in turn is required to calculate the measure $\mathscr{Y}$ as defined by (3.14*b*).

4.2.2. *Magnetic regime* ($\varepsilon_\Lambda \gg \varepsilon_E^2$)

In the large-Δ_E parameter range

$$m^{4/7}E^{3/7} \ll \Lambda \ll E^{1/3} \quad (\Delta_E \gg 1) \tag{4.20a}$$

(equivalently $\varepsilon_\Lambda \gg \varepsilon_E^2$; see (A 2*b*)), the interior layer has a double structure. There is an outer magnetotopographic layer MT_p on the length $\delta_{\Lambda p}$ and an inner Hartmann layer H_p on the length δ_H. Their inverse ratio is

$$\Delta_\Lambda := \frac{\delta_H}{\delta_{\Lambda p}} = \Delta_E^{-7/3} \ll 1. \tag{4.20b}$$

Remember that throughout the parameter range (4.20*a*) the exterior layer is also divided into two such layers of width $\delta_{\Lambda e}$ and δ_H respectively.

(*a*) *Outer magnetotopographic layer*

On the relatively long magnetotopographic MT (compared to the short viscous H) length scales $\delta_{\Lambda p}(\gg \delta_{Ep})$ and $\delta_{\Lambda e}(\gg \delta_{Ee})$, viscous effects are negligible throughout the tangent-cylinder shear layer. This approximation reduces the order of the governing differential equations. So at lowest order we only require continuity of Φ and $\mathrm{d}\Phi/\mathrm{d}x$ for the distinct solutions either side of the tangent cylinder across $x = 0$. Since the interior length $\delta_{\Lambda p}$ is shorter than the exterior length $\delta_{\Lambda e}$, most of the Φ adjustment is made on the exterior *equatorial* side so that its value on the tangent cylinder is almost zero. In consequence, continuity of the first derivative $\mathrm{d}\Phi/\mathrm{d}x$ fixes the Φ amplitude to be of order of the length scale ratio

$$\varepsilon_\Lambda := \frac{\delta_{\Lambda p}}{\delta_{\Lambda e}} = \left(\frac{\Lambda_i H_i}{m}\right)^{1/6}\left(\frac{r_i}{2}\right)^{1/3}\left(\frac{2}{H_i}\right)^{1/2} (\ll 1). \tag{4.21}$$

Accordingly we write

$$\Phi \approx \begin{cases} 1 - (1 - \varepsilon_\Lambda \Phi_M(0))\exp(-\lambda_- x) & \text{for } x \gg \delta_H \\ \varepsilon_\Lambda \Phi_M(x/\delta_{\Lambda p}) & \text{for } -x \gg \delta_H. \end{cases} \tag{4.22}$$

Here we have introduced

$$\Phi_M = \Phi_M(\eta) \quad \text{with } \eta = x/\delta_{\Lambda p}; \tag{4.23a}$$

with this change of variables (3.12*a*) becomes

$$\Delta_\Lambda^2 \frac{\mathrm{d}^4\Phi_M}{\mathrm{d}\eta^4} - \frac{\mathrm{d}}{\mathrm{d}\eta}\left[\left(\Delta_\Lambda \frac{\sigma_i}{(-\eta)^{1/4}} + 1\right)\frac{\mathrm{d}\Phi_M}{\mathrm{d}\eta}\right] - \mathrm{i}\left(\frac{1}{\sqrt{-\eta}} - \varepsilon_\Lambda^2\right)\Phi_M = \mathrm{i}\varepsilon_\Lambda. \tag{4.23b}$$

https://doi.org/10.1017/S0022112099007776 Published online by Cambridge University Press

The problem is complicated by the presence of two independent small parameters Δ_Λ and ε_Λ, whose relative sizes change over the range (4.20*a*). Nevertheless, the biggest correction to the lowest-order solution that we present is $O(\Delta_\Lambda^{1/2})$ and triggered by the Hartmann layer. It remains larger than the $O(\varepsilon_\Lambda)$ corrections throughout the range (4.20*a*) but they are both comparable at the end of the range, where $\varepsilon_\Lambda = O(\Delta_\Lambda^{1/2})$ at $\Lambda = O(E^{1/3})$. Neglecting $O(\Delta_\Lambda)$ terms, (4.23*b*) reduces to

$$\frac{\mathrm{d}^2\Phi_M}{\mathrm{d}\eta^2} + \mathrm{i}\,\frac{\Phi_M}{\sqrt{-\eta}} = -\mathrm{i}\varepsilon_\Lambda, \tag{4.24a}$$

correct to $O(\varepsilon_\Lambda)$. Ignoring, for the moment, any Hartmann boundary layer corrections, continuity of the derivative of (4.22) across $x = 0$ gives

$$\frac{\mathrm{d}\Phi_M}{\mathrm{d}\eta}(0) = \mathrm{e}^{\mathrm{i}\pi/4}(1 - \varepsilon_\Lambda \Phi_M(0)), \tag{4.24b}$$

while boundedness at infinity requires that

$$\Phi_M + \varepsilon_\Lambda\sqrt{-\eta} \to 0 \quad \text{as } \eta \downarrow -\infty. \tag{4.24c}$$

The zeroth-order solution of (4.24*a*) bounded at infinity is

$$\Phi_M = -\mathscr{K}\,\exp\left(-\frac{\mathrm{i}5\pi}{12}\right)\frac{\mathrm{Ai}'(\tau)}{\mathrm{Ai}'(0)}, \qquad \frac{\mathrm{d}\Phi_M}{\mathrm{d}\eta} = -\mathscr{K}2^{1/3}\,\exp\left(\frac{\mathrm{i}\pi}{4}\right)\frac{\mathrm{Ai}(\tau)}{\mathrm{Ai}'(0)}, \tag{4.25a}$$

where $\mathrm{Ai}(\tau)$ is the Airy function, the prime denotes derivative,

$$\tau := 2^{2/3}\exp\left(\frac{-\mathrm{i}\pi}{6}\right)\sqrt{-\eta} \tag{4.25b}$$

and $\mathscr{K} = \mathscr{K}_0$ defined by (B 3*b*) is fixed by the boundary condition (4.24*b*). The next-order solution, which includes the $O(\varepsilon_\Lambda)$ corrections, is outlined in Appendix B.

In order to set up boundary conditions on the thinner Hartmann layer that occurs when $\eta = O(\Delta_\Lambda)$, we need the small-$|\eta|$ expansion of (4.25*a*), namely

$$\Phi_M \sim \Phi_M(0)[1 - \mathrm{i}\,\tfrac{4}{3}(-\eta)^{3/2}] + \frac{\mathrm{d}\Phi_M}{\mathrm{d}\eta}(0)\,\eta[1 - \mathrm{i}\,\tfrac{4}{15}(-\eta)^{3/2}] \quad \text{as } \eta \uparrow 0. \tag{4.26}$$

From a more general point of view, this expansion of the magnetotopographic solution just inside the tangent cylinder shows that the vorticity $-\mathrm{d}^2\Phi/\mathrm{d}x^2$ diverges like $(-x)^{-1/2}$ as $x \uparrow 0$. As a consequence, we are unable to evaluate $\mathscr{L}$ defined by (3.14*b*) from this inviscid solution. The singular behaviour is very similar to that encountered in the magnetic Proudman layers of K-S. In both cases, the effect is caused by relatively strong axial motion linked to the topography. In the axisymmetric case of K-S, it comes about via Ekman suction through the equatorial singularity of the Ekman layer. In our inviscid approximation, Ekman suction has been ignored and the crucial interaction comes from the non-axisymmetric flow over axisymmetric topography – the inner sphere boundary.

(*b*) *Inner Hartmann layer*

The singularity of the outer solution constructed above is removed in an inner Hartmann layer H. In it, though the Ekman suction term remains formally small in the case of rigid boundaries, there is a weak singularity associated with it which adds to the complexity of our problem. Hence to simplify our presentation we restrict attention to the stress-free case

$$\sigma = 0. \tag{4.27}$$

https://doi.org/10.1017/S0022112099007776 Published online by Cambridge University Press

Accordingly we consider the stretched vorticity

$$\Omega_H(\zeta) := -\varepsilon_\Lambda^{-1}\Delta_\Lambda^{-3/2}\delta_H^2\,\frac{\mathrm{d}^2\Phi}{\mathrm{d}x^2} \quad \text{with } \zeta = \frac{x}{\delta_H} \tag{4.28}$$

triggered by the singular vorticity of the outer solution. Correct to leading order it satisfies

$$\frac{\mathrm{d}^2\Omega_H}{\mathrm{d}\zeta^2} - \Omega_H = -\mathrm{i}\,\frac{\Phi_M(0)}{\sqrt{-\zeta}}. \tag{4.29a}$$

Continuity of the second and third derivatives of Φ at $x = 0$ with the exterior Hartmann layer is guaranteed by (4.9*b*). Specifically, at lowest order, we approximate $\lambda_+ = 1/\delta_H$, $\lambda_- = 0$ ($\sigma = 0$) and accordingly (4.9*b*) implies that Ω_H satisfies the boundary conditions

$$\left.\begin{array}{ll} \dfrac{\mathrm{d}\Omega_H}{\mathrm{d}\zeta} + \Omega_H = 0 & \text{at } \zeta = 0, \\ \Omega_H \to 0 & \text{as } \zeta \downarrow -\infty. \end{array}\right\} \tag{4.29b}$$

The solution of the problem (4.29) is

$$\Omega_H = \mathrm{i}\Phi_M(0)\left[\mathrm{e}^{-\zeta}\int_{\sqrt{-\zeta}}^{\infty}\mathrm{e}^{-\rho^2}\mathrm{d}\rho + \mathrm{e}^{\zeta}\int_0^{\sqrt{-\zeta}}\mathrm{e}^{\rho^2}\mathrm{d}\rho\right]. \tag{4.30a}$$

It determines

$$\Omega_H(0) = \mathrm{i}\,\frac{\sqrt{\pi}}{2}\Phi_M(0) \tag{4.30b}$$

and successively (3.14*a*) gives

$$\mathscr{A}_M = -2m\,\frac{\delta_{\Lambda e}}{\delta_H}\Delta_\Lambda^{1/2}\Omega_H(0) = -\mathrm{i}m\sqrt{\pi}\,\frac{\delta_{\Lambda e}}{\delta_H}\Delta_\Lambda^{1/2}\Phi_H(0). \tag{4.31a}$$

In this way, (1.9) reduces with (2.3*d*), (4.25*a*) and (B 3*b*) to

$$\mathscr{Y} = \left|1 + \mathrm{e}^{-\mathrm{i}5\pi/12}\,\frac{6^{1/3}}{4}\Gamma\left(\frac{5}{6}\right)\frac{\delta_{\Lambda e}}{\delta_H}\Delta_\Lambda^{1/2}\left(1 + O(\Delta_\Lambda^{1/2}) + O(\varepsilon_\Lambda)\right)\right|. \tag{4.31b}$$

Note also that integration of (4.29*a*), making use of (4.29*b*), gives

$$\varepsilon_\Lambda^{-1}\Delta_\Lambda^{-3/2}\delta_H\left(\left.\frac{\mathrm{d}\Phi}{\mathrm{d}x}\right|_{x=0} - \frac{\mathrm{d}\Phi}{\mathrm{d}x}\right) = \Omega_H(0) - 2\mathrm{i}\Phi_M(0)\sqrt{-\zeta} + \frac{\mathrm{d}\Omega_H}{\mathrm{d}\zeta}. \tag{4.32}$$

It can be used to quantify the correction to the boundary condition (4.24*b*) on $\mathrm{d}\Phi_M/\mathrm{d}\eta$. First we identify the dominant term at large ζ proportional to $\sqrt{-\zeta}$ with the lowest-order Airy function terms in the solution (4.25*a*) as exhibited by the derivative of (4.26). Then on expressing it in terms of inner variables as $(\delta_{\Lambda p}/\delta_H)^{1/2}\sqrt{-\eta}$, we see that the correction term $\Omega_H(0)$ is smaller by a small factor $O(\Delta_\Lambda^{1/2})$; this is the magnitude of the correction to the boundary condition (4.24*b*) triggered by the Hartmann layer and is incorporated in (4.35) below. This confirms the consistency of our approximation procedure.

(*c*) *Composite solution*

The magnetotopographic and Hartmann layer results can be combined to give the composite solution

$$\Phi \approx \begin{cases} \varepsilon_\Lambda[\Phi_M(x/\delta_{\Lambda p}) - \Delta_\Lambda^{3/2}\Omega_H(x/\delta_H)] & \text{for } x < 0 \\ 1 - [(1 - \varepsilon_\Lambda\Phi_M(0))\,\mathrm{e}^{-\lambda_- x} + \varepsilon_\Lambda\Delta_\Lambda^{3/2}\Omega_H(0)\mathrm{e}^{-\lambda_+ x}] & \text{for } x > 0. \end{cases} \tag{4.33}$$

https://doi.org/10.1017/S0022112099007776 Published online by Cambridge University Press

The combination of terms for $x < 0$ cancels out the algebraic singularities proportional to $(-x)^{3/2}$ present in both Φ_M and Ω_H so giving a uniformly valid lowest-order approximation. From it we may also deduce that the parameters $\alpha_\pm$ in (4.2*a*) are given correct to lowest order by

$$\alpha_- \sim -\varepsilon_\Lambda \Phi_M(0), \qquad 1 + \alpha_+ \sim -\Delta_\Lambda^{1/2} \frac{\sqrt{\pi}}{2} \mathrm{e}^{\mathrm{i}\pi/4} \Phi_M(0). \tag{4.34}$$

Of greater significance is the correction to the value of $\Phi_M(0)$. In particular, the continuity of the derivative of (4.14) at $x = 0$ yields, using (4.29*b*),

$$\frac{\mathrm{d}\Phi_M}{\mathrm{d}\eta}(0) + \Delta_\Lambda^{1/2} \Omega_H(0) = \mathrm{e}^{\mathrm{i}\pi/4} \left(1 - \varepsilon_\Lambda \Phi_M(0)\right). \tag{4.35}$$

Together with (4.30*b*) we obtain the improved approximation

$$\mathscr{K} = \mathscr{K}_0 \Big/ \left[1 - \Delta_\Lambda^{1/2} \frac{\sqrt{\pi}}{2} \mathscr{K}_0 \exp\left(-\frac{\mathrm{i}\pi}{6}\right)\right] + O(\varepsilon_\Lambda) \tag{4.36}$$

for the amplitude if the Airy function solution (4.25*a*).

Of course, a yet higher-order algebraic singularity remains on the tangent cylinder. It is nevertheless weak and manifested by the divergence of the fourth derivative of Φ. That is removed in an ageostrophic $E^{1/3}$-Stewartson layer, as discussed by K-S.

In sumary, the results of this subsection show that

$$\mathscr{Z} = \left|1 - \frac{\sqrt{\pi}}{2} \frac{\delta_{\Lambda e}}{\delta_H} \Delta_\Lambda^{1/2} \Phi_M(0)\right| = O\left(\frac{\Lambda^{5/12}}{m^{1/6} E^{1/4}}\right) \quad \text{for } m^{4/7} E^{3/7} \ll \Lambda \ll E^{1/3}. \tag{4.37}$$

Here the zeroth-order approximation coincides with (4.31*b*); the Hartmann layer $O(\Delta_\Lambda^{1/2})$ correction to $\Phi_M(0)$ is embodied by (4.25*a*) and (4.36), while additional smaller $O(\varepsilon_\Lambda)$ contribution to the solution is outlined in Appendix B and leads to the improved expression (B 4) for $\Phi_M(0)$. The reason for determining these corrections so carefully is two-fold. On the one hand, we wish to establish the consistency of the asymptotic expansions. On the other, we require reliable estimates of the errors when making comparison with the numerical results in § 6. Furthermore, the main conclusion of the quasi-geostrophic approximation employed throughout this section, as it applies to $\Lambda \ll E^{1/3}$, is that the parameter $\mathscr{Z}$ is an increasing function of Λ. When we leave this parameter range, the trend continues but is eventually reversed, as we discuss in the following section.

5. Ageostrophic regime

5.1. *Intermediate regime*

As K-S show – but see also Hollerbach (1996*b*) – the parameter range

$$\Lambda = O(E^{1/3}) \tag{5.1}$$

marks an important transition of flow characteristics which is clearly illustrated by the summary figure 2. As Λ increases to $O(E^{1/3})$, the quasi-geostrophic Hartmann layer width δ_H shrinks to the width $O(E^{1/3})$ of the thinner ageostrophic viscous Stewartson sublayer. As Λ increases beyond $O(E^{1/3})$, a z-dependent magnetogeostrophic layer MG emerges on a broader $O(\Lambda)$ length scale but still small compared to the z-independent magnetotopographic layers MT width $\delta_{\Lambda e}$ and $\delta_{\Lambda p}$. They eventually merge, filling the shell when Λ is $O(1)$. Simultaneously, the Hartmann–Stewartson layer HS contracts

https://doi.org/10.1017/S0022112099007776 Published online by Cambridge University Press

axially to a small stump on the tangent cylinder attached to the equator of the inner sphere. The magnetogeostrophic layer does not completely remove the tangent-cylinder discontinuity. So to determine $\mathscr{Y}$, the Hartmann–Stewartson layer structure needs to be considered.

In order to allow for z-dependence in the flow we write

$$\widetilde{\boldsymbol{u}} \approx \left(\frac{\mathrm{i}m\widetilde{\varphi}}{s} - \frac{\partial \widetilde{\psi}}{\partial z}, -\frac{\partial \widetilde{\varphi}}{\partial s}, \frac{\partial \widetilde{\psi}}{\partial s} \right). \tag{5.2}$$

This representation is approximate in so much as we have neglected azimuthal derivatives of $\widetilde{\psi}$ in comparison with radial derivatives and so the size of m is again limited by (3.2).

A match with the largely z-independent magnetotopographic solution (4.22) is obtained with

$$\widetilde{\varphi} = \varepsilon_{\Lambda} \Phi_M(0) + \mathrm{e}^{\mathrm{i}\pi/4} \frac{x}{\delta_{\Lambda e}} - \mathrm{i} \frac{x^2 - y^2}{2\delta_{\Lambda e}^2} + \mathrm{i}m \left(\frac{2}{r_i} \right)^{1/2} \varepsilon_{\Lambda} \Phi_M(0)\, \varphi(x, z), \tag{5.3a}$$

$$\widetilde{\psi} = -\mathrm{e}^{\mathrm{i}\pi/4} \frac{y}{\delta_{\Lambda e}} + \mathrm{i} \frac{xy}{\delta_{\Lambda e}^2} + \mathrm{i}m \left(\frac{2}{r_i} \right)^{1/2} \varepsilon_{\Lambda} \Phi_M(0)\, \psi(x, z) \tag{5.3b}$$

by the first two linear terms in $\widetilde{\varphi}$. In (5.3a, b), we have introduced

$$y(z) := \frac{\Lambda}{2} \int_0^z \overline{b}_s^2 \Big|_{s=r_i} \mathrm{d}z \quad \text{so that } y(H_i) = \frac{\Lambda_i H_i}{2}, \tag{5.3c}$$

while the functions φ and ψ satisfy

$$2\frac{\partial \psi}{\partial z} = \left(-\Lambda \overline{b}_s^2 + E \frac{\partial^2}{\partial x^2} \right) \frac{\partial \varphi}{\partial x}, \tag{5.4a}$$

$$-2\frac{\partial \varphi}{\partial z} = \left(-\Lambda \overline{b}_s^2 + E \frac{\partial^2}{\partial x^2} \right) \frac{\partial \psi}{\partial x}, \tag{5.4b}$$

which are equivalent to K-S equation (4.3) under appropriate rescalings. In the construction of (5.3), we have arranged the linear and quadratic terms so that they satisfy (5.4) as well as the vanishing of the normal velocity on the outer sphere boundary $r = r_o$, namely $(H_i \partial \widetilde{\psi}/\partial s \approx) \boldsymbol{r} \cdot \boldsymbol{u}_f \approx \mathrm{i}m$ for $|x| \ll 1$. Note also that the y-independent algebraic terms up to $O((x/\delta_{\Lambda e})^2)$ in the expression for $\widetilde{\varphi}$ agree with the expansion of (4.22) for $\delta_{\Lambda e} \gg x > 0$ in the region exterior to the tangent cylinder. In this way, the only non-trivial boundary condition to be met at leading order by our solution of (5.4) stems from the vanishing of the normal velocity on the inner sphere boundary $r = r_i$, namely

$$\mathrm{i}m\widetilde{\varphi} + z_i(s) \frac{\mathrm{d}}{\mathrm{d}s} \widetilde{\psi}(s, z_i(s)) = \boldsymbol{r} \cdot \boldsymbol{u}_f \approx 0$$

for $0 < -x \ll 1$, where as usual $z_i(s) = \sqrt{-2r_i x}$ and $x = s - r_i$. Correct to lowest order integration gives

$$\psi(s, z_i(s)) = (-x)^{1/2}.$$

To the same order of accuracy, we summarize the boundary conditions as follows:

$$\psi = \begin{cases} 0 & \text{on } z = H_i \\ (-x)^{1/2} & \text{on } z = \sqrt{-2r_i x} \quad \text{for } x < 0 \\ 0 & \text{on } z = 0 \quad \text{for } x > 0. \end{cases} \tag{5.5}$$

https://doi.org/10.1017/S0022112099007776 Published online by Cambridge University Press

The pivotal approximation of this section is to assume that the z-length scale is large compared to the inner-sphere boundary height $z_i = \sqrt{-2r_i x}$. On this basis, we apply the inner-sphere boundary condition on $z = 0$; we comment on the range of validity of this approximation at the end of § 5.2.2 and quantify it by (5.26). Accordingly the formal solution of (5.4) subject to (5.5) is

$$\psi(x,z) = \int_{\mathscr{C}_\infty} \widehat{\psi}_0(k)\, \frac{\sinh\left(k\widehat{\chi}(k,z)\right)}{\sinh\left(k\widehat{\chi}_0(k)\right)}\, \mathrm{e}^{\mathrm{i}kx}\, \mathrm{d}k, \tag{5.6a}$$

$$\varphi(x,z) = -\mathrm{i}\int_{\mathscr{C}_\infty} \widehat{\psi}_0(k)\, \frac{\cosh\left(k\widehat{\chi}(k,z)\right)}{\sinh\left(k\widehat{\chi}_0(k)\right)}\, \mathrm{e}^{\mathrm{i}kx}\, \mathrm{d}k + \varphi_0, \tag{5.6b}$$

similar to K-S equation (4.5a, b), where

$$\widehat{\chi}(k,z) := \widehat{\chi}_0(k) - \left(y + \frac{E}{2}\, k^2 z\right), \tag{5.6c}$$

$$\widehat{\chi}_0(k) = \widehat{\chi}(k,0) := \frac{H_i}{2}\left(\Lambda_i + Ek^2\right) \tag{5.6d}$$

and the small constant $\varphi_0 = O((\Lambda_i H_i)^{1/2})$ (see (5.14b) below) is chosen such that $\varphi(0,0) = 0$. Here

$$\widehat{\psi}_0(k) := \frac{1}{4\sqrt{\pi}\,(-\mathrm{i}k)^{3/2}} \tag{5.6e}$$

is analytic in the upper half-plane with the complex plane cut along the negative imaginary axis ($(-\mathrm{i}k)^{3/2} = \mathrm{e}^{-(3/4)\pi \mathrm{i}} k^{3/2}$ for positive real k), while the path of integration also circumvents the origin in the upper half-plane: $\mathscr{C}_\infty := \{x + \mathrm{i}z \mid -\infty < x < \infty,\ z \downarrow 0\}$. Note that (5.6$e$) differs from K-S equation (4.5c) because the algebraic power in our boundary condition (5.5) is $(-x)^{1/2}$ in contrast to $(-x)^{-1/4}$ in K-S equation (4.4).

The most informative feature of this solution is the $z = 0$ value

$$\varphi(x,0) = -\mathrm{i}\int_{\mathscr{C}_\infty} \widehat{\psi}_0(k) \coth\left(k\widehat{\chi}_0(k)\right) \mathrm{e}^{\mathrm{i}kx}\, \mathrm{d}k + \varphi_0. \tag{5.7a}$$

From it, we may deduce the asymptotic results

$$\varphi(x,0) \sim \begin{cases} -\dfrac{4}{3\Lambda_i H_i}\,(-x)^{3/2} & \text{as } x \downarrow -\infty \\ 0 & \text{as } x \uparrow 0 \\ -x^{1/2} & \text{as } x \downarrow 0 \\ \varphi_0 = O((\Lambda_i H_i)^{1/2}) & \text{as } x \uparrow \infty, \end{cases} \tag{5.7b}$$

cf. K-S equation (4.6b). The asymptotic behaviour for $|x| \gg \Lambda_i H_i$ is quasi-geostrophic and matches with the z-independent magnetotopographic solution (4.22). In making this claim, we assume – and establish in (5.14b) below – that φ_0 is negligible in the exterior overlap region $\Lambda_i H_i \ll x \ll \delta_{\Lambda e}$, while the match in the interior overlap region $\Lambda_i H_i \ll -x \ll \delta_{\Lambda p}$ is evident from the expansion (4.26).

The asymptotic behaviour for $|x| \ll \Lambda_i H_i$ is best determined from the asympotic representation (5.18) below in the limit $z \downarrow 0$. The validity of applying the inner-sphere boundary conditions on $z = 0$, as we have done, ceases to be valid for the quadrupole model of H94 once $\Lambda \geqslant O(E^{1/5})$. The necessary refinements appropriate to that case are undertaken in § 6. For the moment, we note that the $-x^{1/2}$ behaviour of $\varphi(x,0)$ as $x \downarrow 0$ is indicative of singularities linked to the equator of the inner sphere. These

https://doi.org/10.1017/S0022112099007776 Published online by Cambridge University Press

are eventually removed in viscous sublayers. A convenient way of quantifying the magnitude of the singularity inside and outside those viscous sublayers is to measure the contribution to $\mathscr{A}_M$ from some height z to the top boundary. From (5.3a) we obtain

$$\mathscr{A}_M(z) := H_i \Lambda \int_z^{H_i} \left[\overline{b}_s^2 \frac{\partial^2 \widetilde{\varphi}}{\partial s^2}\right]_{s=r_i} \mathrm{d}z$$
$$= 2\mathrm{i}m\left[\left(-1+\frac{2y}{\Lambda_i H_i}\right) + H_i\left(\frac{2}{r_i}\right)^{1/2} \varepsilon_\Lambda \Phi_M(0)\,\mathscr{G}(y)\right], \tag{5.8a}$$

$$\mathscr{G}(y) := \int_y^{\Lambda_i H_i/2} \left.\frac{\partial^2 \varphi}{\partial x^2}\right|_{x=0} \mathrm{d}y. \tag{5.8b}$$

The value of $\mathscr{A}_M \equiv \mathscr{A}_M(0)$ determines

$$\mathscr{Z} := \left|H_i\left(\frac{2}{r_i}\right)^{1/2} \varepsilon_\Lambda \Phi_M(0)\,\mathscr{G}(0)\right|, \tag{5.8c}$$

which itself depends on

$$\mathscr{G}(0) = \mathrm{i}\int_{\mathscr{C}_\infty} k^2 \widehat{\psi}_0(k)\left[\int_0^{\Lambda_i H_i/2} \frac{\cosh\left(k\widehat{\chi}(k,z)\right)}{\sinh\left(k\widehat{\chi}_0(k)\right)}\mathrm{d}y\right]\mathrm{d}k. \tag{5.9}$$

In the case of the z-independent radial magnetic field of H94, we can proceed to evaluate $\mathscr{G}(0)$ analytically with

$$2y = \Lambda_i z \quad \text{for model H94.} \tag{5.10}$$

It gives

$$\mathscr{G}(0) = -\frac{\Lambda_i}{4\sqrt{\pi}}\int_{\mathscr{C}_\infty} \frac{\mathrm{d}k}{(-\mathrm{i}k)^{1/2}\left(\Lambda_i + Ek^2\right)} = -\frac{\sqrt{\pi}}{4\,\delta_H^{1/2}} \quad \text{for model H94,} \tag{5.11}$$

where the value of the integral stems from the residue at the pole in the upper half-plane. Together with (5.8c), we recover our earlier results (4.31). The simplicity of this conclusion can be explained by taking the z-average of (5.4a); that recovers (3.12a) for two reasons. First, $\overline{b}_s$ is constant and secondly, we have made the approximation $z_B = 0$, $z_T = H_i$ which implies that we can commute the averaging with the x-partial derivatives.

The main small correction to the result (5.11) stems from applying the inner-sphere boundary condition correctly at $z_i = \sqrt{-2r_i x}$ rather than at $z_i = 0$. In the range $E^{1/3} \ll \Lambda \ll E^{1/5}$, where the result (5.11) is valid, even the magnitude of the correction is difficult to quantify and has not been attempted.

In the case of the dipole model of K-S, we must postpone the evaluation of $\mathscr{G}(0)$ (see (5.23) below) until our detailed analysis of the Hartmann–Stewartson layer in § 5.2.2.

5.2. *Magnetogeostrophic flow and viscous sublayer*

For

$$E^{1/3} \ll \Lambda \ll 1, \tag{5.12}$$

we can distinguish two regions, a magnetogeostrophic layer MG and an internal viscous boundary layer HS attached to the equator of the inner sphere.

https://doi.org/10.1017/S0022112099007776 Published online by Cambridge University Press

5.2.1. *Magnetogeostrophic layer*

On scales sufficiently large that viscous forces can be neglected, the solution of (5.4) subject to (5.5) can be expressed in the complex form

$$\psi + \mathrm{i}(\varphi - \varphi_0) = \frac{1}{4\sqrt{\pi}} \int_{\mathscr{C}_\infty} \frac{\exp\left(\frac{1}{2}\Lambda_i H_i + \mathrm{i}Z\right) k}{(-\mathrm{i}k)^{3/2} \sinh\left(\frac{1}{2}\Lambda_i H_i\, k\right)}\, \mathrm{d}k, \tag{5.13a}$$

$$= -\frac{\mathrm{i}}{\Lambda_i H_i} \int_{-\infty}^{0} \frac{(-X)^{1/2} \exp\left[-\pi(Z-X)/\Lambda_i H_i\right]}{\sinh\left[\pi(Z-X)/\Lambda_i H_i\right]}\, \mathrm{d}X, \tag{5.13b}$$

where Z is an analytic function of the complex variable

$$Z := x + \mathrm{i}\, y = O(\Lambda). \tag{5.13c}$$

The former is simply the Fourier transform solution (5.6) with $E = 0$. The latter alternative form is the Green's function solution, in which the complex Z-plane is cut along the negative real axis of integration. In the right-hand half-plane, the former gives

$$\psi + \mathrm{i}(\varphi - \varphi_0) = \frac{\mathrm{i}}{2^{3/2}\pi} (\Lambda_i H_i)^{1/2} \sum_{n=1}^{\infty} \frac{1}{n^{3/2}} \exp\left(-n \frac{2\pi Z}{\Lambda_i H_i}\right) \quad \text{for } \mathrm{Re}\, Z > 0. \tag{5.14a}$$

So to ensure that $\varphi(0,0) = 0$ we set

$$\varphi_0 = -\frac{\zeta(3/2)}{2^{3/2}\pi} (\Lambda_i H_i)^{1/2} \quad \text{with } \zeta(3/2) \equiv \sum_{n=1}^{\infty} \frac{1}{n^{3/2}}, \tag{5.14b}$$

the Riemann zeta function. In the neighbourhood of the origin the series (5.14*a*) can be summed to give the asymptotic expression

$$\psi + \mathrm{i}\varphi \sim -\mathrm{i}Z^{1/2} \quad \text{for } |Z| \ll \Lambda_i H_i, \tag{5.15}$$

which by analytic continuation is valid for $-\pi < \arg Z < \pi$. It recovers the $x \to 0$ limits in (5.7*b*). The large negative-x behaviour is perhaps best deduced from the Green's function representation (5.13*b*):

$$\left.\begin{aligned} \psi &\sim (-x)^{1/2} \left(1 - \frac{2y}{\Lambda_i H_i}\right) \\ \varphi &\sim -\frac{4}{3\Lambda_i H_i} (-x)^{3/2} \end{aligned}\right\} \quad \text{for } 0 < y < \Lambda_i H_i/2,\ -x \gg \Lambda. \tag{5.16}$$

Here ψ meets the boundary conditions (5.5) on both $z = 0$ and H_i, while φ agrees with the previous result (5.7*b*) on $z = 0$ as $x \downarrow -\infty$.

Since our solution (5.13) of (5.4) with $E = 0$ is potential it is relatively easy to calculate the integral (5.8*b*). It is

$$\mathscr{G}(y) = -\left[\frac{\partial \varphi}{\partial y}\right]_y^{\Lambda_i H_i/2} = -\frac{\partial \psi}{\partial x}(0, H_i) + \left.\frac{\partial \varphi}{\partial y}\right|_{x=0}. \tag{5.17a}$$

The first term is small and can be neglected. So close to the inner sphere, use of (5.15) gives

$$\mathscr{G}(y) = -\frac{1}{2\sqrt{2}}\, y^{-1/2} \quad \text{for } 0 < y \ll \Lambda_i H_i. \tag{5.17b}$$

Since this diverges in the limit $y \downarrow 0$, the reduction to finite values of $\mathscr{G}(0)$ (and

https://doi.org/10.1017/S0022112099007776 Published online by Cambridge University Press

consequently $\mathscr{A}_M$) is accomplished in viscous sublayers attached to the equator of the inner sphere. The failure of the magnetogeostrophic solution to provide a finite value of $\mathscr{A}_M$ has its counterpart in the z-independent case of § 4.2.2(a).

5.2.2. *Hartmann–Stewartson layer*

On the short length scales, where viscous forces are important, the solution (5.6) reduces at leading order to

$$\psi = \int_{-\infty}^{\infty} \widehat{\psi}_0(k)\, \mathrm{e}^{\Xi}\, \mathrm{d}k, \qquad \varphi = -\mathrm{i} \int_{-\infty}^{\infty} \frac{|k|}{k} \widehat{\psi}_0(k)\, \mathrm{e}^{\Xi}\, \mathrm{d}k, \tag{5.18a}$$

where

$$\Xi := \mathrm{i}kx - |k|y - \tfrac{1}{2}E|k|^3 z. \tag{5.18b}$$

In evaluating (5.18a), we regard $|k|$ as an analytic function except for cuts along both imaginary axes excluding the origin $k = 0$ of the complex k-plane, through which the contour of integration passes. From this representation we can determine the small-$|x|$ asymptotic behaviour in (5.7b). That form itself is interesting as it essentially removes the singular behaviour of $\partial\widetilde{\psi}/\partial s$ inside the tangent cylinder leaving the stronger part outside.

The size of the (viscous) Hartmann–Stewartson layer stumps, described by (5.18a), may be estimated on the basis that the three terms on the right-hand side of (5.18b), which contribute to Ξ, are comparable. It gives

$$x \sim y \sim (Ez)^{1/3}. \tag{5.19}$$

Let us define the height δ_{HS} of the stump to be that value of z at which the inviscid value, namely $\mathscr{A}_M(\delta_{HS})$ (5.8a) with (5.17b), agrees with the viscous value $\mathscr{A}_M$. For the uniform radial field case with $\mathscr{G}(0)$ given by (5.11), we obtain

$$\delta_{HS} = \frac{2}{\pi}\frac{\delta_H}{\Lambda_i} = \frac{2}{\pi}\left(\frac{E}{\Lambda_i^3}\right)^{1/2} \quad \text{for model H94,} \tag{5.20}$$

consistent with the length scale estimate $\Lambda_i \delta_{HS} = O((E\delta_{HS})^{1/3})$ required by (5.19).

In the case of the dipole model of K-S, it is first necessary to determine $\mathscr{A}_M$ on the basis that its dominant contribution comes from the viscous stump. So under the approximations made in (5.18), the formula (5.9) reduces to

$$\mathscr{G}(0) = -\frac{1}{4\sqrt{\pi}} \int_{-\infty}^{\infty} \frac{|k|}{(-\mathrm{i}k)^{1/2}} \left[\int_0^{\infty} \exp\left(-|k|y - \tfrac{1}{2}E|k|^3 z\right) \mathrm{d}y\right] \mathrm{d}k, \tag{5.21a}$$

in which correct to lowest order we have

$$y \approx \frac{\Lambda_{ei}}{6r_i^2} z^3 \quad \text{with } \Lambda_{ei} := \Lambda r_i^2 \left(\frac{\partial \overline{b}_s}{\partial z}\right)^2 (r_i, 0) \tag{5.21b}$$

(cf. K-S equation (4.13), remembering that there $\overline{\boldsymbol{b}}$ is a potential field). With the change of variables

$$z = \left(\frac{\Lambda_{ei}}{6r_i^2}\right)^{-3/8} \left(\frac{2}{E}\right)^{-1/8} \varpi, \qquad k = \left(\frac{\Lambda_{ei}}{6r_i^2}\right)^{1/8} \left(\frac{2}{E}\right)^{3/8} \varpi K, \tag{5.22a}$$

the double integral (5.21a) becomes

$$\mathscr{G}(0) \sim -\frac{3}{4\sqrt{\pi}} \left(\frac{4\Lambda_{ei}}{3r_i^2 E^3}\right)^{1/16} \int_{-\infty}^{\infty} \int_0^{\infty} \frac{|K| \exp\left[-(|K| + |K|^3)\varpi^4\right]}{(-\mathrm{i}K)^{1/2}} \varpi^{7/2}\, \mathrm{d}\varpi\, \mathrm{d}K, \tag{5.22b}$$

https://doi.org/10.1017/S0022112099007776 Published online by Cambridge University Press

where $|K|$ and $(-\mathrm{i}K)^{1/2}$ as functions of K have the same properties in the complex plane as k. Successive integrations with respect to ϖ and K respectively yield

$$\mathscr{G}(0) \sim -\frac{3}{8\sqrt{2\pi}}\,\Gamma\left(\frac{9}{8}\right)\left(\frac{4\Lambda_{ei}}{3r_i^2E^3}\right)^{1/16}\int_0^\infty \frac{K^{-5/8}}{\left(1+K^2\right)^{9/8}}\,\mathrm{d}K,$$

$$= -\frac{3}{16\sqrt{2\pi}}\,\Gamma\left(\frac{3}{16}\right)\Gamma\left(\frac{15}{16}\right)\left(\frac{4\Lambda_{ei}}{3r_i^2E^3}\right)^{1/16} \quad \text{for model K-S.} \tag{5.23}$$

It determines the boundary layer height

$$\delta_{HS} = \left(\frac{8\sqrt{\pi}}{3\,\Gamma(3/16)\,\Gamma(15/16)}\right)^{2/3}\left(\frac{6r_i^2}{\Lambda_{ei}}\right)^{3/8}\left(\frac{E}{2}\right)^{1/8} \quad \text{for model K-S.} \tag{5.24}$$

In summary the boundary layer height for both the quadrupole and dipole models is consistently a function of $\Lambda/E^{1/3}$:

$$\delta_{HS} = \begin{cases} O\left(\left[\dfrac{\Lambda}{E^{1/3}}\right]^{-3/2}\right) & \text{for model H94} \\ O\left(\left[\dfrac{\Lambda}{E^{1/3}}\right]^{-3/8}\right) & \text{for model K-S.} \end{cases} \tag{5.25}$$

The latter is, of course, consistent with (5.19) and recovers the stump dimensions given by K-S equation (4.15).

Finally, we check the consistency of the assumption that the sphere boundary height $\sqrt{-2r_ix}$, with $x = O((E\delta_{HS})^{1/3})$, is small compared to the stump boundary layer height δ_{HS}. This scale separation is required to justify the assumption that the sphere boundary condition can be applied on $z = 0$ and is satisfied only when

$$r_i^3E \ll \delta_{HS}^5. \tag{5.26}$$

For model H94 it is only met when $\Lambda \ll E^{1/5}$, as shown schematically on figure 2. In contrast, for model K-S it is met throughout the range $\Lambda \ll 1$, as assumed by K-S, and figure 2 must be modified accordingly.

Our results for $\mathscr{G}(0)$ provide us with the following estimates of the size of $\mathscr{Z}$ given by (5.8*c*):

(i) For the uniform field model, our result (5.11) shows that (4.37) continues to hold and so subject to the requirement (5.26), we have

$$\mathscr{Z} = O\left(\frac{\Lambda^{5/12}}{m^{1/6}E^{1/4}}\right) \quad \text{throughout } E^{1/3} \ll \Lambda \ll E^{1/5} \quad \text{for model H94.} \tag{5.27}$$

We consider the appropriate modifications necessary for larger values of $\Lambda\,(\geqslant O(E^{1/5}))$ in the following section.

(ii) For the dipole model, the result (5.23) determines

$$\mathscr{Z} = O\left(\frac{\Lambda^{11/48}}{m^{1/6}E^{3/16}}\right) \quad \text{throughout } E^{1/3} \ll \Lambda \ll 1 \quad \text{for model K-S.} \tag{5.28}$$

The actual asymptotic value is determined from (5.8*c*), (5.21*b*) and (5.23).

https://doi.org/10.1017/S0022112099007776 Published online by Cambridge University Press

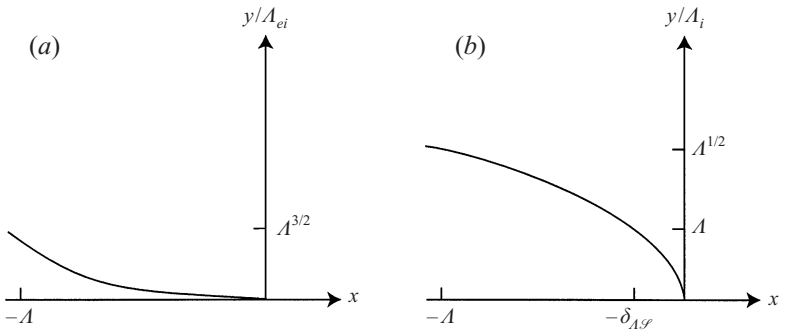


FIGURE 3. The location of the inner-sphere boundary in the stretched x, y-space. (a) For the dipole magnetic field K-S the boundary is cusped; $y_i^2 = -2\Lambda_{ei}^2 x^3/9r_i$. ($b$) For the quadrupole magnetic field H94 the boundary is elliptical; $y_i^2 = -\Lambda_i^2 r_i x/2$.

6. Model H94

Throughout this section we restrict attention to model H94 for which $y = \Lambda_i z/2$ (see (5.10)) and in consequence the inner-sphere boundary $\mathscr{S}$ is located at $y = y_i(s)$:

$$y_i := \frac{\Lambda_i z_i}{2} = 2\sqrt{-\delta_{\Lambda\mathscr{S}} x} \quad \text{with } \delta_{\Lambda\mathscr{S}} := \frac{\Lambda_i^2 r_i}{8} \tag{6.1}$$

for $0 \leqslant -x = O(\delta_{\Lambda\mathscr{S}})$ and illustrated in figure 3(b) (the corresponding plot for model K-S is shown in figure 3(a) for comparison). Our primary interest is the influence of the boundary location on the flow in the neighbourhood of the equator to the inner sphere on the radial s-scale $O(\Lambda^2)$ and corresponding axial z-scale $O(\Lambda)$ identified by (6.1). As noted in (5.26), when

$$\Lambda = O(E^{1/5}) \quad \text{equivalently } \Delta_{\mathscr{S}} = O(1), \tag{6.2a}$$

where

$$\Delta_{\mathscr{S}} := \frac{\delta_H}{\delta_{\Lambda\mathscr{S}}}, \tag{6.2b}$$

the z-scale δ_{HS} of the Hartmann–Stewartson layer stump given by (5.25) is $O(\Lambda)$ too. So in this parameter range the analysis of that layer given in § 5.2 ceases to be valid, because the inner-sphere boundary condition can no longer be applied on $z = 0$.

To resolve the true nature of the resulting equatorial region, we need to consider the outer magnetogeostrophic layer MG and the inner Hartmann–Stewartson layer HS taking proper account of the location of the inner-sphere boundary and its associated Ekman–Hartmann surface layer. Their relative sizes depend on whether $\Delta_{\mathscr{S}}$ is large or small. When $E^{1/3} \ll \Lambda \ll E^{1/5}$ ($\Delta_{\mathscr{S}} \gg 1$), the surface layer is an $E^{1/2}$-Ekman layer thickening to an $E^{2/5}$-equatorial Ekman layer EE of axial extent $O(E^{1/5})$ contained within the Hartmann–Stewartson layer stump, as illustrated in figure 4. When $\Lambda = O(E^{1/5})$, the stump collapses into the surface layer, which for $E^{1/5} \ll \Lambda \ll 1$ ($\Delta_{\mathscr{S}} \ll 1$) re-emerges as an $(E/\Lambda)^{1/2}$-equatorial Hartmann layer EH of circumferential extent $O(\Lambda)$, as illustrated in figure 5.

In the subsections below, we address the nature of the magnetogeostrophic flow in § 6.1, solve the Ekman–Hartmann layer equations for $\Delta_{\mathscr{S}} \ll 1$ in § 6.2.1 and discuss briefly the form of the Hartmann–Stewartson layer for $\Delta_{\mathscr{S}} \gg 1$ in § 6.2.2. Then in § 6.3 we summarize our findings for the strength $\mathscr{I}$ of the tangent cylinder singularity for the entire range $\Lambda \ll 1$.

https://doi.org/10.1017/S0022112099007776 Published online by Cambridge University Press

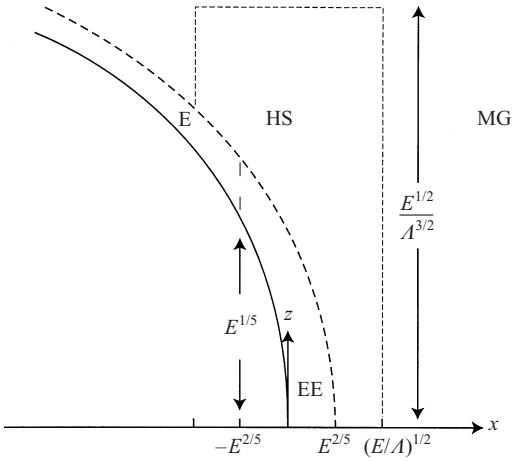


FIGURE 4. The dimensions of the Hartmann–Stewartson stump (HS), Ekman (E) and the equatorial Ekman (EE) layers for model H94, when $E^{1/3} \ll \Lambda \ll E^{1/5}$. All boundaries are marked by broken lines. These layers are surrounded externally by the magnetogeostrophic (MG) layer.

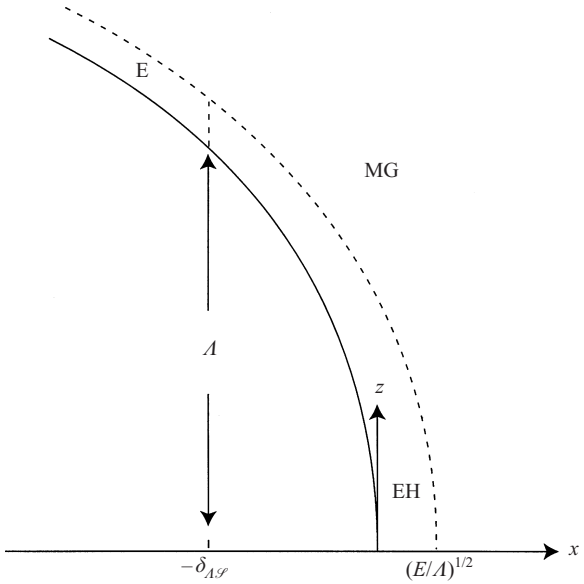


FIGURE 5. As in figure 4, when $E^{1/5} \ll \Lambda \ll 1$ except that the HS and EE layers have merged into a single equatorial Hartmann (EH) layer.

6.1. *Magnetogeostrophic flow*

The magnetogeostrophic solution of (5.4) with $E = 0$ is, of course, potential so that we can continue to express $\psi + \mathrm{i}\varphi$ as an analytic function of $Z := x + \mathrm{i}y$. The solution which satisfies (5.5) on the inner-sphere boundary $\mathscr{S}$ defined by (6.1) and matches with (5.15) in the overlap region $\delta_{\Lambda\mathscr{S}} \ll |Z| \ll \Lambda_i H_i$ is

$$\psi + \mathrm{i}\varphi = \psi_{\mathscr{M}} + \mathrm{i}\varphi_{\mathscr{M}} := \mathrm{i}[\sqrt{\delta_{\Lambda\mathscr{S}}} - (Z + \delta_{\Lambda\mathscr{S}})^{1/2}], \tag{6.3a}$$

https://doi.org/10.1017/S0022112099007776 Published online by Cambridge University Press

where we have used the property

$$(Z+\delta_{\Lambda\mathscr{S}})^{1/2} = \sqrt{\delta_{\Lambda\mathscr{S}}} + \mathrm{i}\,(-x)^{1/2} \quad \text{on } \mathscr{S}. \tag{6.3b}$$

Interestingly it removes the singularity at the origin exhibited by the far-field solution (5.15) and shows that radial s-scale of the solution is never less than $O(\delta_{\Lambda\mathscr{S}})$ in the fluid region.

The removal of the singularity has striking consequences with regard to our measure $\mathscr{A}_M(z)$, defined by (5.8a). For upon use of (6.3), the value (5.17a) of the integral (5.8b) is

$$\mathscr{G}(y) = \mathscr{G}_{\mathscr{M}}(y) := -\frac{[\sqrt{y^2+\delta_{\Lambda\mathscr{S}}^2} - \delta_{\Lambda\mathscr{S}}]^{1/2}}{2\sqrt{2}\,\sqrt{y^2+\delta_{\Lambda\mathscr{S}}^2}}. \tag{6.4a}$$

So unlike the earlier result (5.17b), which diverges as $y \downarrow 0$, the new limit is zero; $\mathscr{G}(0) = 0$. More precisely, it exhibits the asymptotic behaviour

$$\mathscr{G}_{\mathscr{M}}(y) \sim \begin{cases} -\dfrac{1}{2\sqrt{2}}\, y^{-1/2} & \text{for } y \gg \delta_{\Lambda\mathscr{S}} \\ -\dfrac{1}{4\sqrt{2}}\, \delta_{\Lambda\mathscr{S}}^{-1/2} & \text{at } y = \sqrt{3}\delta_{\Lambda\mathscr{S}} \\ -\dfrac{1}{4}\,\dfrac{y}{\delta_{\Lambda\mathscr{S}}^{3/2}} & \text{for } y \ll \delta_{\Lambda\mathscr{S}}, \end{cases} \tag{6.4b}$$

where we have included the local minimum value at $y = \sqrt{3}\delta_{\Lambda\mathscr{S}}$.

The above result is very revealing as it shows a reversed sign contribution to $\mathscr{A}_M$ near the equator of the inner sphere, which reduces the size of $\mathscr{A}_M(z)$, once z decreases below $(\sqrt{3}/4)r_i\Lambda_i$. Of crucial importance in determining the realized value of $\mathscr{A}_M$ is the location of the viscous cut-off $z = \delta_{HS}$. Essentially, it says that as the width of the viscous boundary layer shrinks so does $\mathscr{A}_M$; the structure of that layer is discussed below.

6.2. *Viscous sublayer*

6.2.1. *Equatorial Hartmann layer* ($\Delta_{\mathscr{S}} \ll 1$)

Here we restrict attention to the small-$\Delta_{\mathscr{S}}$ limit

$$E^{1/5} \ll \Lambda \ll 1 \tag{6.5}$$

and investigate the nature of the equatorial Hartmann layer EH of width δ_H attached to the surface of the inner sphere near its equator $x = z = 0$. This shellular layer only intersects the tangent cylinder for a height $O((r_i\delta_H)^{1/2})$ above the equator so determining the domain of influence on the value of $\mathscr{A}_{\mathscr{M}}$. To the order of accuracy attempted here our modus operandi is to simply add to the magnetogeostrophic solution (6.3) the approriate boundary layer correction.

For the case of stress-free boundaries employed by H94, we require the radial derivative of the tangential velocity to vanish on the inner sphere $\mathscr{S}$. According to (5.2) at lowest order that requires the vorticity to vanish:

$$\left.\frac{\partial^2\psi}{\partial x^2}\right|_{\mathscr{S}} = 0, \qquad \left.\frac{\partial^2\varphi}{\partial x^2}\right|_{\mathscr{S}} = 0. \tag{6.6}$$

On the other hand, the magnetogeostrophic values determined by (6.3) and (6.1) are

$$\left.\frac{\partial^2\psi_{\mathscr{M}}}{\partial x^2}\right|_{\mathscr{S}} + \mathrm{i}\left.\frac{\partial^2\varphi_{\mathscr{M}}}{\partial x^2}\right|_{\mathscr{S}} = \frac{\mathrm{i}}{4\delta_{\Lambda\mathscr{S}}^{3/2}}\left[1 + \mathrm{i}\,\frac{\Lambda_i z}{4\delta_{\Lambda\mathscr{S}}}\right]^{-3/2}. \tag{6.7}$$

https://doi.org/10.1017/S0022112099007776 Published online by Cambridge University Press

The non-zero value of the vorticity, implied by (6.7), in the magnetogeostrophic flow is brought to zero across a Hartmann layer in which we set

$$\frac{\partial^2\psi}{\partial x^2} = \frac{1}{4\delta_{\Lambda\mathscr{S}}^{3/2}}\,\mathscr{P}, \qquad \frac{\partial^2\varphi}{\partial x^2} = \frac{1}{4\delta_{\Lambda\mathscr{S}}^{3/2}}\,\mathscr{Q}, \tag{6.8a}$$

which we partition into magnetogeostrophic ($\mathscr{M}$) and Hartmann ($\mathscr{H}$) contributions

$$\mathscr{P} := \mathscr{P}_{\mathscr{M}} + \mathscr{P}_{\mathscr{H}}, \qquad \mathscr{Q} := \mathscr{Q}_{\mathscr{M}} + \mathscr{Q}_{\mathscr{H}}. \tag{6.8b}$$

Here the magnetogeostrophic part is given by the second x-derivative of (6.3a), namely

$$\mathscr{Q}_{\mathscr{M}} - \mathrm{i}\mathscr{P}_{\mathscr{M}} = (1 + \mathrm{i}2\sqrt{\Delta_{\mathscr{S}}}Y + \Delta_{\mathscr{S}}X)^{-3/2}, \tag{6.9a}$$

where

$$X = \frac{x}{\delta_H}, \qquad Y = \frac{y}{2\sqrt{\delta_{\Lambda\mathscr{S}}\delta_H}}. \tag{6.9b}$$

For small $\Delta_{\mathscr{S}}$, the Binomial expansion of (6.9a) yields

$$\mathscr{P}_{\mathscr{M}} = 3\Delta_{\mathscr{S}}^{1/2}\,Y + O(\Delta_{\mathscr{S}}^{3/2}), \qquad \mathscr{Q}_{\mathscr{M}} = 1 - \frac{3\Delta_{\mathscr{S}}}{2}(X + 5Y^2) + O(\Delta_{\mathscr{S}}^2). \tag{6.9c}$$

Substitution of (6.8a) into (5.4) shows that

$$\left(\frac{\partial^2}{\partial X^2} - 1\right)\frac{\partial\mathscr{Q}}{\partial X} = \frac{\Delta_{\mathscr{S}}^{1/2}}{2}\,\frac{\partial\mathscr{P}}{\partial Y}, \tag{6.10a}$$

$$\left(\frac{\partial^2}{\partial X^2} - 1\right)\frac{\partial\mathscr{P}}{\partial X} = -\frac{\Delta_{\mathscr{S}}^{1/2}}{2}\,\frac{\partial\mathscr{Q}}{\partial Y}, \tag{6.10b}$$

where according to (6.7)

$$\mathscr{P} = 0, \quad \mathscr{Q} = 0 \quad \text{on the boundary } \mathscr{S}: \quad Y = \sqrt{-X}. \tag{6.11}$$

Since the third-order X-derivatives of $\mathscr{P}_{\mathscr{M}}$ and $\mathscr{Q}_{\mathscr{M}}$ are so small, their contribution to (6.10) can be neglected. Under that approximation $\mathscr{P}_{\mathscr{H}}$ and $\mathscr{Q}_{\mathscr{H}}$ satisfy (6.10), whose solution satisfying the boundary condition (6.11), is

$$\mathscr{P}_{\mathscr{H}} = \widehat{\mathscr{P}}_{\mathscr{H}}\exp\left[-(X + Y^2)\right], \qquad \mathscr{Q}_{\mathscr{H}} = \widehat{\mathscr{Q}}_{\mathscr{H}}\exp\left[-(X + Y^2)\right], \tag{6.12a}$$

where

$$\widehat{\mathscr{P}}_{\mathscr{H}} = -\Delta_{\mathscr{S}}^{1/2}Y\left[3 + \tfrac{1}{2}(X + Y^2)\right] + O\left(\Delta_{\mathscr{S}}^{3/2}\right),$$

$$\widehat{\mathscr{Q}}_{\mathscr{H}} = -1 + \Delta_{\mathscr{S}}\{6Y^2 + \tfrac{1}{8}[(Y^2 - \tfrac{1}{2})(X + Y^2)^2 + (13\,Y^2 - \tfrac{15}{2})(X + Y^2)]\} + O(\Delta_{\mathscr{S}}^2). \tag{6.12b}$$

We now express (5.8b), namely

$$\mathscr{G}(y) = \mathscr{G}_{\mathscr{M}}(y) + \mathscr{G}_{\mathscr{H}}(y), \tag{6.13a}$$

as the sum of the magnetogeostrophic contribution (6.4) and the Hartmann layer contribution $\mathscr{G}_{\mathscr{H}}(y)$. The $y = 0$ value

$$\mathscr{G}(0) = \mathscr{G}_{\mathscr{H}}(0) = \frac{\sqrt{\delta_H}}{2\delta_{\Lambda\mathscr{S}}}\int_0^\infty \mathscr{Q}_{\mathscr{H}}|_{X=0}\,\mathrm{d}Y \qquad (\mathscr{G}_{\mathscr{M}}(0) = 0) \tag{6.13b}$$

https://doi.org/10.1017/S0022112099007776 Published online by Cambridge University Press

is evaluated using the expansion (6.12); in turn (5.8*a*) yields

$$\mathscr{A}_M + 2\mathrm{i}m = -2\mathrm{i}m\left(\frac{2}{r_i}\right)^{3/2}\frac{H_i\sqrt{\pi\delta_H}}{\Lambda_i^2}\,\varepsilon_\Lambda \mathscr{Y}(\Delta_\mathscr{S})\Phi_M(0), \tag{6.14a}$$

where

$$\mathscr{Y}(\Delta_\mathscr{S}) = \frac{2}{\sqrt{\pi}}\int_0^\infty \mathscr{Q}_\mathscr{H}|_{X=0}\,\mathrm{d}Y = 1 - \tfrac{63}{16}\Delta_\mathscr{S} + O(\Delta_\mathscr{S}^2). \tag{6.14b}$$

Significantly, we can also establish from (6.12) that

$$\frac{2}{\sqrt{\pi}}\int_0^\infty \left.\frac{\partial^2 \mathscr{Q}_\mathscr{H}}{\partial x^2}\right|_{X=0}\mathrm{d}Y = \mathscr{Y}(\Delta_\mathscr{S}) + O(\Delta_\mathscr{S}^2). \tag{6.14c}$$

It is consistent up to $O(\Delta_\mathscr{S})$ with (1.8*a*) and (2.4*b*) which require

$$\mathscr{A}_M + \mathscr{A}_v = -2\mathrm{i}m. \tag{6.14d}$$

6.2.2. *Hartmann–Stewartson layer and* $\Delta_\mathscr{S} \gg 1$

Let us briefly recap the situation for large $\Delta_\mathscr{S}$, as it may be deduced directly from the problem (6.10), (6.11). For though its complete solution is not readily obtained, we may, as in § 5, take advantage of the long Y length scale and apply the inner-sphere boundary condition on $Y = 0$. We, therefore, integrate (6.10*a*) from $Y = 0$ to ∞ and use the boundary values of $\mathscr{P}_\mathscr{H}$ at $z = 0$ and H_i to obtain

$$\left(\frac{\partial^2}{\partial X^2} - 1\right)\left[\int_0^\infty \mathscr{Q}_\mathscr{H}\,\mathrm{d}Y\right] = \begin{cases} \dfrac{1}{\Delta_\mathscr{S}(-X)^{1/2}} & \text{for } X < 0 \\ 0 & \text{for } X > 0 \end{cases} \qquad (\Delta_\mathscr{S} \gg 1). \tag{6.15}$$

Its solution, undertaken in § 4.2.2(*b*), leads to the result (4.31), which we noted via (5.11) continues to hold in the range $E^{1/3} \ll \Lambda \ll E^{1/5}$ appropriate here.

In summary, (4.31) and (6.14) imply that

$$\mathscr{Z} = \begin{cases} \dfrac{\sqrt{\pi}H_i}{\Lambda_i r_i}\,\varepsilon_\Lambda \Delta_\mathscr{S}^{-1/2}\,|\Phi_M(0)| & \text{for } E^{3/7} \ll \Lambda \ll E^{1/5} \\ \dfrac{\sqrt{\pi}H_i}{\Lambda_i r_i}\,\varepsilon_\Lambda \Delta_\mathscr{S}^{1/2}\mathscr{Y}(\Delta_\mathscr{S})\,|\Phi_M(0)| & \text{for } E^{1/5} \ll \Lambda \ll 1. \end{cases} \tag{6.16}$$

The interesting aspect of our results for $E^{1/5} \ll \Lambda \ll 1$ is that $\mathscr{Z}$ decreases as Λ increases, a point which is more readily seen from (6.19) below. Also of note is the fact the value of $\mathscr{Z}$ is of order unity (again see (6.19)) when $\Lambda = O(E^{3/25})$ and thereafter $E^{3/25} \ll \Lambda \ll 1$ is small. Nevertheless, the most important feature of the two asymptotic results (6.16) is that they are of the same order of magnitude, when $\Delta_\mathscr{S} = O(1)$ (i.e. $\Lambda = O(E^{1/5})$).

Clearly at fixed small E, the maximum $\mathscr{Z}_{max}$ of $\mathscr{Z}$ and its location $\Lambda = \Lambda_{max}$ occurs when $\Delta_\mathscr{S} = O(1)$. The determination of their exact values, therefore, requires the solution of the boundary layer problem (6.10), (6.11) when $\Delta_\mathscr{S} = O(1)$. Since that substantial task has not been undertaken, we simply note that under the lowest-order approximation $\mathscr{Y}(0) = 1$, the maximum value of $\mathscr{Z}$ predicted by equality on each range in (6.16) is

$$\mathscr{Z} = \frac{\sqrt{\pi}H_i}{\Lambda_i r_i}\,\varepsilon_\Lambda\,|\Phi_M(0)| \tag{6.17a}$$

https://doi.org/10.1017/S0022112099007776 Published online by Cambridge University Press

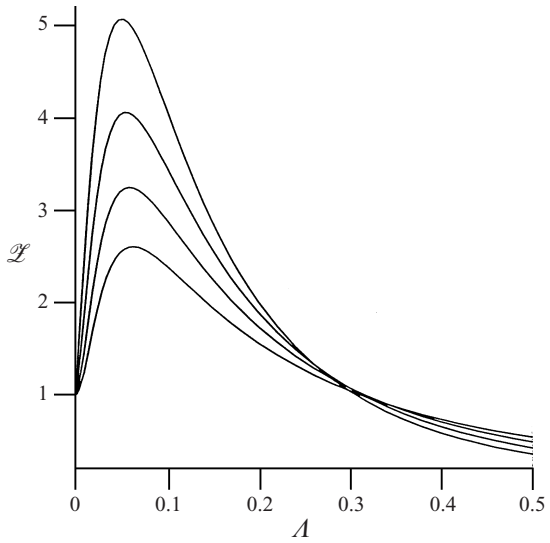


FIGURE 6. Numerical results for the measure $\mathscr{L}$ plotted vs. Λ at fixed $E = 10^{-4.0}$, $10^{-4.5}$, $10^{-5.0}$ and $10^{-5.5}$. Each case is identified by its local maximum $\mathscr{L}_{max}$ at Λ_{max}, as itemized in table 1. The maxima shown increase with decreasing E.

which occurs when

$$\Delta_{\mathscr{S}} = 1. \tag{6.17b}$$

Of course, this happens outside the range of validity of both asymptotic values. Even more seriously, the power series (6.14*b*) for $\mathscr{Y}(\Delta_{\mathscr{S}})$ has clearly failed at $\Delta_{\mathscr{S}} = 1$ very badly! The estimate (6.17*a*) is therefore likely to considerably overestimate the true maximum value $\mathscr{L}_{max}$ and likewise (6.17*b*) provides an unreliable estimate of its location Λ_{max}. Only the orders of magnitude can be trusted from a quantitative viewpoint.

6.3. *Comparison with numerical results*

The parameter values employed by H94 are

$$\left.\begin{array}{llll} r_i = \frac{1}{2}, & r_o = \frac{3}{2}, & H_i = \sqrt{2}, & m = 1, \\ \delta_{Ee} = E^{1/4}, & \delta_{Ep} = \dfrac{E^{2/7}}{2^{1/7}}, & \varepsilon_E = \dfrac{E^{1/28}}{2^{1/7}}, & \Delta_E = \dfrac{\Lambda^{1/2}}{2^{1/7}E^{3/14}}, \\ \delta_{\Lambda e} = \Lambda^{1/2}, & \delta_{\Lambda p} = \dfrac{\Lambda^{2/3}}{2^{1/3}}, & \varepsilon_\Lambda = \dfrac{\Lambda^{1/6}}{2^{1/3}}, & \Delta_\Lambda = \dfrac{2^{1/3}E^{1/2}}{\Lambda^{7/6}}, \\ \Lambda_i = \Lambda, & \delta_{\Lambda\mathscr{S}} = \dfrac{\Lambda^2}{16}, & \delta_H = \dfrac{E^{1/2}}{\Lambda^{1/2}}, & \Delta_{\mathscr{S}} = \dfrac{16E^{1/2}}{\Lambda^{5/2}}. \end{array}\right\} \tag{6.18}$$

Further numerical evaluations of $\mathscr{L}$, as a function of Λ, at four small distinct values of E have been undertaken and the results are illustrated in figure 6. The general trends agree well with our asymptotic predictions (4.8) and (6.16) for the parameter

https://doi.org/10.1017/S0022112099007776 Published online by Cambridge University Press

E	$10^{-4.0}$	$10^{-4.5}$	$10^{-5.0}$	$10^{-5.5}$
$\mathscr{Z}_{max}$	2.61	3.25	4.06	5.09
Λ_{max}	0.064	0.061	0.057	0.053

TABLE 1. The value of $\mathscr{Z}_{max}$ and Λ_{max} for the numerical results portrayed in figure 6.

values (6.18):

$$\mathscr{Z} \sim \begin{cases} \left[1+\sqrt{2}\,\dfrac{\Lambda}{E^{1/2}}+\dfrac{\Lambda}{E}\right]^{1/2}+O\left(E^{1/28}\right) & \text{for } \Lambda \leqslant O(E^{1/2}), \\ \dfrac{\Lambda}{E^{1/2}}\left[1+O\left(\dfrac{\Lambda^{1/2}}{E^{3/14}}\right)\right] & \text{for } E^{1/2} \ll \Lambda \ll E^{3/7}, \\ 2^{2/3}\sqrt{2\pi}\,\mathscr{K}_0\,\dfrac{\Lambda^{5/12}}{4E^{1/4}}\left[1+O\left(\dfrac{E^{1/4}}{\Lambda^{7/12}}\right)\right] & \text{for } E^{3/7} \ll \Lambda \leqslant O(E^{1/3}), \\ 2^{2/3}\sqrt{2\pi}\,\mathscr{K}_0\,\dfrac{\Lambda^{5/12}}{4E^{1/4}} & \text{for } E^{1/3} \ll \Lambda \ll E^{1/5}, \\ 2^{2/3}\sqrt{2\pi}\,\mathscr{K}_0\,\dfrac{4E^{1/4}}{\Lambda^{25/12}}\left[1-63\,\dfrac{E^{1/2}}{\Lambda^{5/2}}+O\left(\dfrac{E}{\Lambda^5}\right)\right] & \text{for } E^{1/5} \ll \Lambda \ll 1, \end{cases} \tag{6.19}$$

where $\mathscr{K}_0$ is defined by (B 3*b*). The errors itemized are $O(\varepsilon_E)$, $O(\Delta_E)$ (see (4.19)) and $O(\Delta_{\mathscr{S}})$ (see (6.14)) respectively.

The numerically determined maximum values $\mathscr{Z}_{max}$ are itemized in table 1. For comparison, our asymptotic estimated 'maximum', where the lowest-order values of the last two entries of (6.19) coincide (see (6.17)), is

$$\mathscr{Z} = \sqrt{\pi}\,\mathscr{K}_0\,(2E)^{-1/6} \quad \text{occurring at } \Lambda = 2^{8/5}E^{1/5}, \tag{6.20}$$

a formula which substantially overestimates Λ_{max}. Furthermore, if we include the correction term in the expression for the last entry, we see that the resulting expression achieves a local maximum at

$$\Lambda = \left(\frac{693}{5}\right)^{2/5} E^{1/5}. \tag{6.21}$$

Now, even for $E = 10^{-5.5}$, the smallest value employed in the numerics, the realized value is $\Lambda \approx 0.57$, which is about 10 times too large. A more reassuring feature of the numerical results is that $\mathscr{Z}_{max}$ appears to scale as $E^{-0.194}$ which is close to the analytic prediction $E^{-1/6}$.

The correction terms and error estimates in (6.19) are very illuminating. They clearly explain why we cannot expect quantitative agreement with the numerics in the range of parameters employed. On the one hand, for small $\Lambda = O(E^{1/2})$ the error terms $O(E^{1/28})$ are only negligible when E is extremely small. On the other, for relatively large $\Lambda = O(E^{1/5})$ we still need to reduce E by several orders of magnitude before the value of Λ mentioned in (6.21) is numerically small and only for values of Λ large compared to that is the last entry of (6.19) likely to be reliable.

https://doi.org/10.1017/S0022112099007776 Published online by Cambridge University Press

7. Conclusions

Our analytic development has extended K-S's earlier study of axisymmetric shear layers on the tangent cylinder to the non-axisymmetric case. In that respect the most significant finding is the nature of the new quasi-geostrophic shear layers important in the range $\Lambda \ll E^{1/3}$. In contrast, the asymmetry of the flow does not influence the ageostrophic boundary layer structures, which gain importance for larger field strengths $E^{1/3} \ll \Lambda \ll 1$. Nevertheless, we emphasize that the axial length scale of the Hartmann–Stewartson layers attached to the equator of the inner sphere is controlled by the strength of the local radial field $\overline{b}_s$ there. So whereas $\overline{b}_s|_{z=0}$ vanishes for the dipole parity of K-S, it is non-zero for the quadrupole parity of H94. In that case, the stronger equatorial magnetic field quenches the shear more effectively and consequently the Hartmann–Stewartson layer evaporates once Λ exceeds $E^{1/5}$. Since these results do not depend on asymmetry, our analysis of § 6 of model H94 also applies to the axisymmetric version of K-S's problem with quadrupole field.

The motivation for the present study stemmed from H94's numerical results, which have been extended here and illustrated in figure 6 to provide a clear picture of the strength $\mathscr{Z}$ of the tangent cylinder singularity. The increase in $\mathscr{Z}$ at low Λ visible in the figure is consistent with the quasi-geostrophic analytic results. Though one might expect that, once Λ exceeded $E^{1/3}$ and the flow is magnetogeostrophic almost everywhere, the confinement of the shear into relatively small viscous layers would eliminate the singularity, it is not, however, the case. Instead, while the Hartmann–Stewartson layer stump attached to the equator of the inner cylinder has a finite size, there are strong shears located in it that continue to increase the realized value of $\mathscr{Z}$. For magnetic fields with dipole parity that state of affairs continues for all $\Lambda \ll 1$; we can only speculate that $\mathscr{Z}$ decreases with further increase of Λ.

For the quadrupole parity state of H94, the analytic results paint a clearer picture. The finite radial magnetic field removes much of the singular behaviour of the magnetogeostrophic flow near the equator of the inner sphere and the Hartmann–Stewartson layer stump disappears when $\Lambda = O(E^{1/5})$. There only remains a weak singularity associated with the equatorial Hartmann layer. Though it is only possible to make analytic progress in the range $E^{1/5} \ll \Lambda \ll 1$, the asymptotics of § 6.2.1 clearly highlight the structure of that layer and identify what contributes to the value of $\mathscr{Z}$, which now decreases with Λ. The local maximum identified tentatively by (6.21) cannot be taken seriously and only provides a rather generous quantification of a lower bound on Λ at which the expansion breaks down. As pointed out in § 6.2.2, the solution of the boundary layer problem for $\Delta_{\mathscr{S}} = O(1)$ is also needed in order to identify the behaviour near the maximum of $\mathscr{Z}$ and to obtain any possible quantitative agreement with the numerics.

We should stress that the detailed nature of the results of § 6.2.1, which are central to comparison with the numerical results, depend on the inner-sphere boundary being slippery. In the rigid case we must replace (6.6) with no-slip boundary conditions, which presumably at the very least alter the powers of $\Delta_{\mathscr{S}}$ in the expansions of the solution.

As in K-S, a very complicated nesting of boundary layers exists on the tangent cylinder in the various parameter ranges considered, as illustrated schematically in figure 2. We have been careful to check the consistency of our scaling laws by taking the asymptotic solutions beyond lowest order where possible. The delicate nature of the ordering and scaling is emphasized by the narrow parameter bands in (6.19). Evidently for $\Lambda \ll E^{1/5}$, the error terms in (6.19) are only small for extremely small

https://doi.org/10.1017/S0022112099007776 Published online by Cambridge University Press

numerical values of E. At first sight, $E^{1/5} \ll \Lambda \ll 1$ would appear to be a promising range for quantitative comparison with the numerical results illustrated in figure 6. Unfortunately the large coefficient 63 in (6.19) again limits the validity of the results to values of E smaller than those employed. We, therefore, conclude that though the analytic results are consistent with the numerical results, smaller values of E are required to obtain quantitative agreement.

We thank Mike Proctor and anonymous referees for helpful comments. The support of both PPARC grant numbers GR/K06495 and GR/L40922 is gratefully acknowledged.

Appendix A. The key length scales and parameter ratios

Here we summarize the key parameters. We begin with the length scales outside and inside the tangent cylinder:

$$\left.\begin{aligned} \delta_{Ee} &:= \left(\frac{EH_i}{m}\right)^{1/4}\left(\frac{H_i}{2}\right)^{1/4}, & \delta_{\Lambda e} &:= \left(\frac{\Lambda_i H_i}{m}\right)^{1/2}\left(\frac{H_i}{2}\right)^{1/2}, \\ \varepsilon_E\delta_{Ee} = \delta_{Ep} &:= \left(\frac{EH_i}{m}\right)^{2/7}\left(\frac{r_i}{2}\right)^{1/7}, & \varepsilon_\Lambda\delta_{\Lambda e} = \delta_{\Lambda p} &:= \left(\frac{\Lambda_i H_i}{m}\right)^{2/3}\left(\frac{r_i}{2}\right)^{1/3}, \\ \varepsilon_E &:= \left(\frac{EH_i}{m}\right)^{1/28}\left(\frac{r_i}{2}\right)^{1/7}\left(\frac{2}{H_i}\right)^{1/4}, & \varepsilon_\Lambda &:= \left(\frac{\Lambda_i H_i}{m}\right)^{1/6}\left(\frac{r_i}{2}\right)^{1/3}\left(\frac{2}{H_i}\right)^{1/2}. \end{aligned}\right\} \tag{A 1}$$

They are related to the Hartmann length scale by

$$\frac{\delta_{Ep}^{7/4}}{\delta_{\Lambda p}^{3/4}} = \frac{\delta_{Ee}^2}{\delta_{\Lambda e}} = \delta_H := \left(\frac{E}{\Lambda_i}\right)^{1/2}, \tag{A 2a}$$

which in turn, yields

$$\Delta_E^{1/3} = \Delta_\Lambda^{-1/7} = \frac{\varepsilon_\Lambda}{\varepsilon_E^2} = \left(\frac{\Lambda_i^{1/3}}{E^{1/7}}\right)^{1/2}\left(\frac{r_i H_i^2}{2m^2}\right)^{1/21}, \tag{A 2b}$$

where

$$\Delta_E := \frac{\delta_{Ep}}{\delta_H}, \quad \Delta_\Lambda := \frac{\delta_H}{\delta_{\Lambda p}}. \tag{A 2c}$$

The H94 model with stress-free boundaries also involves

$$\delta_{\Lambda\mathscr{S}} := \frac{\Lambda_i^2 r_i}{8}, \quad \Delta_{\mathscr{S}} = \frac{\delta_H}{\delta_{\Lambda\mathscr{S}}}. \tag{A 3}$$

The Ekman suction associated with rigid boundaries involes the parameters

$$\sigma_o = \left(\frac{r_o}{2mH_i}\right)^{1/2}, \quad \sigma_i = \left(\frac{r_i}{2mH_i}\right)^{1/2}. \tag{A 4}$$

Appendix B. Higher-order magnetotopographic corrections

Here we extend the analysis of § 4.2.2(*a*) of the outer magnetogeostrophic layer and outline the $O(\varepsilon_\Lambda)$ corrections to the solution of the problem (4.24). To achieve this

https://doi.org/10.1017/S0022112099007776 Published online by Cambridge University Press

aim, we also incorporate the Hartmann jump condition and replace the boundary condition (4.24*b*) by (4.35). With (4.30*b*) it gives

$$\frac{\mathrm{d}\Phi_M}{\mathrm{d}\eta}(0) + \mathrm{i}\Delta_A^{1/2}\frac{\sqrt{\pi}}{2}\Phi_M(0) = \mathrm{e}^{\mathrm{i}\pi/4}(1-\varepsilon_A\Phi_M(0)). \tag{B 1}$$

The solution of (4.24*a*) subject to the boundedness condition (4.24*c*) is

$$\left.\begin{aligned}\Phi_M + \varepsilon_A\sqrt{-\eta} &= -\mathscr{K}\,\exp\left(-\frac{\mathrm{i}5\pi}{12}\right)\frac{\mathrm{Ai}'(\tau)}{\mathrm{Ai}'(0)} - \varepsilon_A\,\frac{\pi}{2^{2/3}}\,\exp\left(\frac{\mathrm{i}\pi}{6}\right)\mathrm{Gi}'(\tau),\\ \frac{\mathrm{d}\Phi_M}{\mathrm{d}\eta} &= -\mathscr{K}\,2^{1/3}\exp\left(\frac{\mathrm{i}\pi}{4}\right)\frac{\mathrm{Ai}(\tau)}{\mathrm{Ai}'(0)} - \varepsilon_A\,\frac{\pi}{2^{1/3}}\,\exp\left(\frac{5\mathrm{i}\pi}{6}\right)\mathrm{Gi}(\tau),\end{aligned}\right\} \tag{B 2a}$$

in which $\mathscr{K}$ is a constant, yet to be determined, τ is defined by (4.25*b*) and $\mathrm{Gi}(\tau)$ is closely related to the Airy function:

$$\mathrm{Ai}(\tau) := \frac{1}{\pi}\int_0^\infty \cos\left(\frac{\rho^3}{3}+\tau\rho\right)\mathrm{d}\rho \quad\text{and}\quad \mathrm{Gi}(\tau) := \frac{1}{\pi}\int_0^\infty \sin\left(\frac{\rho^3}{3}+\tau\rho\right)\mathrm{d}\rho \tag{B 2b}$$

(see Abramowitz & Stegun 1965, § 10.4).

Evaluation of (B 2*a*) at $\eta = 0$ in conjunction with the boundary condition (B 1) gives

$$\left.\begin{aligned}\Phi_M(0) &= -\mathscr{K}\,\exp\left(-\frac{\mathrm{i}5\pi}{12}\right) - \varepsilon_A\,\frac{\mathscr{K}_0\mathscr{K}_1}{2}\,\exp\left(\frac{\mathrm{i}\pi}{6}\right),\\ 1-\left[\varepsilon_A + \Delta_A^{1/2}\frac{\sqrt{\pi}}{2}\exp\left(-\frac{\mathrm{i}\pi}{4}\right)\right]\Phi_M(0) &= \exp\left(-\frac{\mathrm{i}\pi}{4}\right)\frac{\mathrm{d}\Phi_\mathrm{M}}{\mathrm{d}\eta}(0) = \frac{\mathscr{K}}{\mathscr{K}_0} + \varepsilon_A\,\frac{\mathscr{K}_1}{2}\,\exp\left(-\frac{5\mathrm{i}\pi}{12}\right),\end{aligned}\right\} \tag{B 3a}$$

where

$$\left.\begin{aligned}\mathscr{K}_0 &:= -\frac{\mathrm{Ai}'(0)}{2^{1/3}\mathrm{Ai}(0)} = \left(\frac{3}{2}\right)^{1/3}\frac{\Gamma(2/3)}{\Gamma(1/3)} = \frac{6^{1/3}}{2\sqrt{\pi}}\,\Gamma\left(\frac{5}{6}\right) = 0.57862\ldots,\\ \mathscr{K}_1 &:= \frac{2^{2/3}\pi}{3^{1/2}}\,\mathrm{Ai}(0) = \frac{\Gamma(1/3)}{3^{2/3}2^{1/3}} = 1.08626\ldots.\end{aligned}\right\} \tag{B 3b}$$

They determine

$$\Phi_M(0) = -\mathscr{K}_0\exp\left(-\frac{\mathrm{i}5\pi}{12}\right)\frac{1-\varepsilon_A\mathscr{K}_1\exp\left(\dfrac{-\mathrm{i}5\pi}{12}\right)}{1-\mathscr{K}_0\left[\varepsilon_A\exp\left(\dfrac{-\mathrm{i}5\pi}{12}\right)+\Delta_A^{1/2}\dfrac{\sqrt{\pi}}{2}\exp\left(-\dfrac{\mathrm{i}\pi}{6}\right)\right]}. \tag{B 4}$$

REFERENCES

Abramowitz, M. & Stegun, A. 1965 *Handbook of Mathematical Functions*. Dover.

Anufriev, A. P. & Hejda, P. 1998 Effect of the magnetic field at the inner core boundary on the flow in the Earth's core. *Phys. Earth Planet. Inter.* **106**, 19–30.

Anufriev, A. P. & Hejda, P. 1999 Are axially symmetrical models of the dynamo adequate for modelling the geodynamo? *Phys. Earth Planet. Inter.* **111**, 69–74.

Aurnou, J., Brito, D. & Olson, P. 1996 Mechanics of inner core super-rotation. *Geophys. Res. Lett.* **23**, 3401–3404.

https://doi.org/10.1017/S0022112099007776 Published online by Cambridge University Press

Busse, F. H. & Cuong, P. G. 1977 Convection in rapidly rotating fluid shells. *Geophys. Astrophys. Fluid Dyn.* **8**, 17–41.

Christensen, U., Olson, P. & Glatzmaier, G. A. 1998 A dynamo model interpretation of geomagnetic field structures. *Geophys. Res. Lett.* **25**, 1565–1568.

Dormy, E., Cardin, P. & Jault, D. 1998 MHD flow in a slightly differentially rotating spherical shell, with conducting inner core, in a dipolar magnetic field. *Earth Planet. Sci. Lett.* **160**, 15–30.

Fearn, D. R. 1997 The geodynamo. In *Earth's Deep Interior* (ed. D. J. Crossley), pp. 79–114. Gordon and Breach.

Glatzmaier, G. A. & Roberts, P. H. 1995*a* A three-dimensional convective dynamo solution with rotating and finitely conducting inner core and mantle. *Phys. Earth Planet. Inter.* **91**, 63–75.

Glatzmaier, G. A. & Roberts, P. H. 1995*b* A three-dimensional self-consistent computer simulation of a geomagnetic reversal. *Nature* **377**, 203–209.

Glatzmaier, G. A. & Roberts, P. H. 1996*a* An anelastic evolutionary geodynamo simulation driven by compositional and thermal convection. *Physica* D **97**, 81–94.

Glatzmaier, G. A. & Roberts, P. H. 1996*b* The rotation and magnetism of Earth's inner core. *Science* **274**, 1887–1891.

Glatzmaier, G. A. & Roberts, P. H. 1997 Simulating the geodynamo. *Contemp. Phys.* **38**, 269–288.

Greenspan, H. P. 1968 *The Theory of Rotating Fluids*. Cambridge University Press.

Hollerbach, R. 1994*a* Magnetohydrodynamic Ekman and Stewartson layers in a rotating spherical shell. *Proc R. Soc. Lond.* A **444**, 333–346.

Hollerbach, R. 1994*b* Imposing a magnetic field across a nonaxisymmetric shear layer in a rotating spherical shell. *Phys. Fluids* **6**, 2540–2544 (referred to herein as H94).

Hollerbach, R. 1996*a* On the theory of the geodynamo. *Phys. Earth Planet. Inter.* **98**, 163–185.

Hollerbach, R. 1996*b* Magnetohydrodynamic shear layers in a rapidly rotating plane layer. *Geophys. Astrophys. Fluid Dyn.* **82**, 237–253.

Hollerbach, R. & Proctor, M. R. E. 1993 Non-axisymmetric shear layers in a rotating spherical shell. In *Theory of Solar and Planetary Dynamos* (ed. M. R. E. Proctor, P. C. Matthews & A. M. Rucklidge), pp. 145–152. Cambridge University Press.

Kitauchi, H. & Kida, S. 1998 Intensification of magnetic field by concentrate-and-stretch of magnetic flux lines. *Phys. Fluids* **10**, 457–468.

Kleeorin, N., Rogachevskii, I., Ruzmaikin, A., Soward, A. M. & Starchenko, S. 1997 Axisymmetric flow between differentially rotating spheres in a dipole magnetic field. *J. Fluid Mech.* **344**, 213–244 (referred to herein as K-S).

Kuang, W. & Bloxham, J. 1997 An Earth-like numerical dynamo model. *Nature* **389**, 371–374.

Kuang, W. & Bloxham, J. 1999 Numerical modelling of magnetohydrodynamic convection in a rapidly rotating spherical shell: Weak and strong field dynamo action. *J. Comput. Phys.* **153**, 51–81.

Sakuraba, A. & Kono, M. 1999 Effect of the inner core on the numerical solution of the magnetohydrodynamic dynamo. *Phys. Earth Planet. Inter.* **111**, 105–121.

Sarson, G. R., Jones, C. A. & Longbottom, A. W. 1998 Convection driven geodynamo models of varying Ekman number. *Geophys. Astrophys. Fluid Dyn.* **88**, 225–259.

Sarson, G. R. & Jones, C. A. 1999 A convection driven geodynamo reversal model. *Phys. Earth Planet. Inter.* **111**, 3–20.

Song, X. & Richards, P. G. 1996 Seismological evidence for differential rotation of the Earth's inner core. *Nature* **382**, 221–244.

Stewartson, K. 1957 On almost rigid rotations. *J. Fluid Mech.* **3**, 299–303.

Stewartson, K. 1966 On almost rigid rotations. Part 2. *J. Fluid Mech.* **26**, 131–144.

Taylor, J. B. 1963 The magneto-hydrodynamics of a rotating fluid and the Earth's dynamo problem. *Proc R. Soc. Lond.* A **274**, 274–283.

https://doi.org/10.1017/S0022112099007776 Published online by Cambridge University Press